FGFR4 regulates tumor subtype differentiation in luminal breast cancer and metastatic disease

Supplemental Material / Methodology

1. Methodology

Animal studies

All animal procedures were performed in accordance with protocols approved by the Institutional Animal Care and Use Committee (IACUC) at University of North Carolina. The WHIM11 PDX was originally obtained from Washington University in St. Louis and is called Washington University Human In Mice (WHIM) tumors. Sample handling and xenograft procedures using WHIM11 have been described in Usary et al(1). Briefly, tumors were engrafted in the mammary fat pad of NSG (NOD.Cg-*Prkdc*^{scid} *Il2rg*^{tm1Wjl}/SzJ) mice (The Jackson Laboratory) by subcutaneous injection of 1.0×10^6 PDX cells in RPMI:Matrigel (BD Biosciences, San Jose, CA) (1:1) in a total volume of 200 µl. For therapeutic testing, tumors were allowed to progress to a diameter of 0.5-0.7 cm and tumor-bearing mice were assigned at random to one of three groups: no treatment (control), BLU9931 treatment, or Lapatinib treatment. Mice receiving therapy were regularly fed with BLU9931 (0.6g of drug/kg/day, Selleckchem) or Lapatinib (0.22g of drug/kg/day, Novartis) diet chow (Research Diets Inc., New Brunswick, NJ) for 18 days. Tumor volume was regularly measured with a caliper and calculated as tumor volume = (length x width^2) x π/ 6. At day 18, treatment studies were complete and mice were euthanized in accordance with institutional guidelines for sample collection. Tumors were recovered and frozen in liquid nitrogen and stored at -80°C until RNA extraction.

Cell lines

The following cell lines were purchased from American Type Culture Collection and were cultured according to their instructions. MDA-MB-453, CAMA-1 and T47D are derived from metastatic carcinoma pericardial effusion and MCF7 derived from adenocarcinoma pleural effusion. Cell cultures were incubated at 37ºC in a humidified 5% CO_2 atmosphere. All cell lines were maintained in complete growth media (corresponding media supplemented with a mix of penicillin/streptomycin plus fungizone (ratio 9:1) at 1% (GIBCO-ThermoFisher Scientific), 1% of L-GlutaMAX™ 200 mM and 10% of fetal bovine serum (FBS) (Sigma-Aldrich, St. Louis, MO). For estrogen starvation experiments (in MCF7 and T47D cell lines), we used phenol-red free DMEM media (GIBCO-ThermoFisher Scientific, Hampton, NH) with 5% of Charcoal stripped fetal bovine serum (Sigma-Aldrich, St. Louis, MO) with a mix of penicillin/streptomycin plus fungizone (ratio 9:1) at 1% (GIBCO-ThermoFisher Scientific, Hampton, NH), and 1% of L-GlutaMAX™ 200 mM.

Cell viability assays

The CellTiter 96 Aqueous One Solution Cell Proliferation Assay Kit (MTS, Promega) was used to determine the rate of cell proliferation. Sub-confluent cultures of the CAMA-1 and MDA-MB453 cell lines were established by seeding a 96 well plate at a density of 10,000 cells/well, allowing cells to attach overnight. Next, cells were treated with the FGFR4 inhibitor BLU9931 diluted in DMSO (from 0 to 20µM) for 48 hours in complete growth media. Cells were monitored daily and after 48 hours 20 µl of MTS were added to each well and the cells were incubated for 1-2 hours in a humidified, 5% CO_2 atmosphere. Absorbance was measured using a Synergy HTX microplate spectrophotometer (Biotek, Winooski, VT) at 490 nm and reference/background was measured at 690 nm. Cells treated with DMSO were used as a control and results were normalized to 100% of viability. Thus, the viability of cells receiving each treatment was calculated relative to controls. In all cases, the corresponding dose of DMSO (never above 0.01% v/v) was added to the control points (dose 0). The half maximal inhibitory concentration (IC50 was calculated with GraphPad Prism® 5.0 software. The IC50 doses were assessed in sextuplicate and every experiment was done at least twice.

Inhibition of FGFR4 in breast cancer cell lines with BLU9931

To inhibit FGFR4 signaling, cells cultured until 70% confluence with complete growth media and then treated with BLU9931 for 48 hours according to the calculated IC50: 2.5 μM (MDA-MB-453) or 10 μM (CAMA-1). After treatment, cells were washed twice with cold PBS and then lysed for RNA. The experiments with each cell line were repeated at least four times to ensure reproducibility of results and all quantitative data was generated from four or more replicates.

Protein measurement and Immunoblot analysis

For protein extraction, cells were lysed in ice-cold radioimmunoprecipitation lysis and extraction buffer (RIPA) and halt protease and phosphatase inhibitor single-use cocktail following manufacturing instructions (ThermoFisher Scientific, Hampton, NH). After 5 minutes of centrifugation at 13000 rpm, supernatants were quantified for protein content using the Lowry method (DC™ Protein Detergent-compatible colorimetric assay Kit II and the protein standard II assay) from Biorad (Hercules, CA) to create a standard curve, both form BioRad. Equal amounts of proteins (70 μg) were separated by Mini-PROTEAN® TGX™ Precast Gels (BioRad) and electrophoretically transferred to polyvinylidene difluoride (PVDF) membranes (BioRad) and blocked with Odyssey® Blocking Buffer (LI-COR, Lincoln, NE) for 1 hour. Membranes were incubated overnight at 4°C with FGF Receptor 4 (D3B12) XP® Rabbit mAb (#8562-Cell signaling, Danvers, MA) in Odyssey Blocking Buffer (TBS)+0.2% Tween® 20 (1:1000 dilution each) (LI-COR, Lincoln, NE). To confirm equal protein loading, membranes were incubated with β-Actin Mouse mAb (#8H10D10-Cell signaling, Danvers, MA) as internal control. After washing three times for 3 to 5 minutes in 1X TBS-T (0.1% Tween 20), membranes were incubated one hour with IRDye® 800CW Donkey anti-Rabbit IgG secondary antibodies (P/N: 926-32213) form LI-COR (Lincoln, NE). Visual of proteins were detected with Odyssey® imaging system (LI-COR, Lincoln, NE). The Image Studio™ Software was used for the quantification of each protein. Correct Mr was compared with prestained protein standards (BioRad).

Kinase enrichment using multiplexed inhibitor beads (MIBs)

Flash frozen tumors were pulverized and lysed using a mortar and pestle in MIBs lysis buffer (50mM HEPES, pH 7.5, 150mM NaCl, 0.5% Triton X-100, 1mM EDTA, 1mM EGTA, 10mM NaF, 2.5mM NaVO4, protease inhibitor cocktail (Roche, Basel, Switzerland), and phosphatase

inhibitor cocktails 2 and 3 (Sigma-Aldrich, St. Louis, MO)). Lysates were sonicated and clarified by centrifugation at 16,000 x g. Supernatants were filtered through 0.2 µm syringe filter and protein concentration determined by Bradford protein assay. Protein concentrations were adjusted to 1 mg/mL in 3 mL of MIBs lysis buffer prior to adjusting salt concentration to 1M NaCl. Columns consisting of 163 µl of settled multiplexed inhibitor beads (MIB) composed of 6 immobilized kinase inhibitors (1x; PP58, Purvalanol B, UNC-21474A, BKM120, UNC-8088A and (1.5x) VI-16832) were equilibrated with MIBs high salt buffer (50mM HEPES, pH 7.5, 1M NaCl, 0.5% Triton X-100, 1mM EDTA, 1mM EGTA). Lysates were then passed over the MIB columns by gravity flow and columns washed sequentially with MIBs high salt buffer, MIBs low salt buffer (50mM HEPES, pH 7.5, 1M NaCl, 0.5% Triton X-100, 1mM EDTA, 1mM EGTA), and MIBs low salt buffer with 0.1% SDS. Bound proteins were eluted by boiling in 100mM Tris-HCl, pH 6.8, 0.5% SDS, and 1% β-mercaptoethanol. DL-DTT was added to a final concentration of 5mM and samples were incubated at 60°C for 25 minutes. Samples were cooled to room temperature and iodoacetamide was added to a final concentration of 20 mM. Samples were incubated for 30 minutes in the dark before DL-DTT concentration was adjusted to 10mM and incubated for 5 more minutes in the dark. Samples were then concentrated to ~100µL using Amicon Ultra centrifugal concentrators and proteins purified by methanol chloroform extraction. Protein pellets were resuspended in 50mM HEPES, pH 8.0 and digested with sequencing grade porcine trypsin (Promega, Madison, WI) overnight at 37°C. Samples were then extracted with hydrated ethyl acetate 3 times to remove residual detergent and desalted using Pierce C-18 spin columns according to the manufacturer's protocol.

LC/MS/MS Analysis

Samples were analyzed by LC-MS/MS using a Thermo Easy nLC 1200 coupled to an Orbitrap QExactive HF mass spectrometer equipped with an Easy Spray nano source. Samples were injected onto an Easy Spray HPLC column (75 µm ID X 25 cm, 2 µm particle size) and eluted over a 120-minute method. The gradient for separation consisted of 5-40% B at a flow rate of 250 nL/minute where mobile phase A was water with 0.1% formic acid and B was 80% acetonitrile with 0.1% formic acid. The QExactive HF was operated in data-dependent mode where the 15 most intense precursors were selected for fragmentation. Resolution for the precursor scan (m/z 350-1700) was set to 120,000 with a target value of 3 × 106 ions, 100 ms

max IT. MS/MS scan resolution was set to 15,000 with a target value of 1 × 105 ions, 75 ms max IT. Normalized collision energy was set to 27% for HCD. Dynamic exclusion was set to 30 s and precursors with unknown charge or charge state of 1 and ≥ 8 were excluded.

MS data analysis

Raw files were processed using the MaxQuant software suite (version 1.6.2.10) with integrated Andromeda search engine against a target-decoy database using human and mouse Uniprot/Swiss-prot proteomes. A maximum of two missed tryptic cleavages were allowed and fixed modifications included carbamidomethylation of cysteine residues. Variable modifications specified were oxidation of methionine and acetylation of N-termini. Ambiguous mouse/human proteins were classified as human. Results were filtered to a 1% FDR at the unique peptide level. Proteins levels were quantified across all samples using MaxLFQ (Max label-free quantification) software(2). Matching between runs was allowed using a four minute match time window and 20 minute alignment time window. Label-free quantification (LFQ)required > 1 unique peptide. Lastly, we used the COMBAT method (3) to correct the batch effect of the log2 transformed LFQ intensity values between experiments. After batch correction the data was median centered and two-class Significance Analysis of Microarrays (SAM)(4, 5) from 'samr' package in R was used to identify differently captured kinases/proteins at FDR of 5%.

Lentiviral infections

The FGFR4 nucleotide sequence was cloned into the lentiviral transfer mammalian vector pLOC containing a dual marker cassette: a nuclear localized TurboGFP™ for easy tracking and a Blasticidin S-resistance gene for selection. FGFR4 gene and the dual cassette was separated by an IRES element to allow the expression of FGFR4 and TurboGFP™/Blasticidin S resistance genes in a single transcript. Lentiviral particles pLOC-TurboGFP-FGFR4 (#OHS6088) and pLOCTurbo-RFP (#OHS5833) (named empty vector or control) were purchased from Dharmacon (Horizon Discovery, Cambridge, UK). MCF7 and T47D cells were transduced with lentiviral particles plus hexadimethrine bromide to a final concentration of up to 8 μg/ml in reduced serum media (DMEM or RPMI-1640, respectively; 5% Fetal Bovine Serum; 2 mM L-glutamine; 1x Penicillin/Streptomycin) and incubated for 18-20 hours at 37°C in a humidified incubator in an atmosphere of 5% CO2. The selection of positive clones was performed by

antibiotic selection with Blasticidin (GIBCO-ThermoFisher Scientific, Hampton, NH) (10 μg/ml) in complete growth medium for at least 2 weeks followed by an additional enrichment by Fluorescent Activated Cell Sorting (FACS).

Live/Dead cell viability assay

MCF7 or T47D (control) and MCF7-FGFR4 or T47D-FGFR4 cells were seeded using complete growth media. After 24 hours, cells were either estrogen-deprived for 6 days using phenol-red-free DMEM and 5% of charcoal-stripped serum or were grown in complete media (phenol-red-free DMEM with 10% of FBS). FGFR4-GFP and control cells grown with whole FBS or estrogen-deprived medium were trypsinized, washed and preincubated for 15 minutes with cold HBSS+1% FBS. For each condition, $1x10^6$ of cells resuspended in 1ml of HBSS were incubated with 1 μl of LIVE/DEAD™ Fixable Violet Dead Cell Stain Kit (Excitation⁄Emission: 416⁄451 nm) (#L34955 - TermoFisher Scientific, Hampton, NH) for 30 minutes protected from light. Cells were then washed three times in HBSS +1% FBS and incubated for 15 minutes at room temperature in 100 μL of 2% paraformaldehyde. Finally, cells were washed once with 1 mL of HBSS +1% FBS, resuspended in 300 μL of HBSS and analyzed by flow cytometry using a BD LSRFortessa™ cell analyzer.

Fluorescence activated cell sorting (FACS)

Cells were first enriched by antibiotic selection. For FACS, FGFR4-GFP cells or control vector-GFP-RFP were trypsinized, washed and preincubated for 15 minutes with cold PBS+1% FBS. FGFR4-GFP and control cells were incubated with a PE anti-human CD334 (FGFR4) (#324306) and PE Mouse IgG1, κ Isotype Control (FC) (#400113) from Biolegend (San Diego, CA) at 1:100 dilution in a DAPI (#62248) form Thermofisher Scientific (Hampton, NH) (0.5μg/ml)-PBS+1% FBS buffer at 4°C for 30 min. Cells were then washed three times in PBS+1% FBS and resuspended in sorting buffer (EDTA 1mM, HEPES 25mM and FBS 1%). Cell sorting was performed on a BD Biosciences FACSAria III cell sorter. Cells without staining were used to determine the settings of autofluorescence. DAPI positive cells were considered non-viable and removed during sorting experiments. Live cells were gated on the basis of forward and side scatter, and single cells were gated on the basis of side and forward scatter height (SSC-H and FSC-H) vs side and forward scatter area (SSC-A and FSC-A), respectively. Gates were

determined by analysis of stained and single cells FGFR4+/GFP+ (cells overexpressing FGFR4-GFP) or RFP+/GFP+ (cells infected with the control vector also referred as "empty vector"). Cells were collected in DMEM or RPMI+5% FBS and plated. Cell sorting was repeated twice.

Isolation and quantification of RNA

Cell line lysate was prepared using QIAshredder tubes (QIAGEN, Hilden, Germany). Tumor tissue was disrupted using roto-stator homogenization. RNA was isolated using the RNeasy Mini Kit (QIAGEN, Hilden, Germany) according to manufacturer protocol. Isolated RNA was quantified using a NanoDrop® Spectrophotometer.

Microarray-Based Gene-Expression Analysis

DNA microarrays protocol was performed as described in Hu et al(6, 7). For tumor and cell line studies, 1 μg of total RNA sample of untreated, BLU9931 treated, or Lapatinib treated tumors were compared to 1 μg of total RNA common reference (human universal, Stratagene). Total RNA was amplified and labeled using Agilent's Low RNA Input Linear Amplification Kit (#5190-0444) from Agilent Technologies (Santa Clara, CA). RNA labeling tumor (Cy5 CTP) and reference (Cy3 CTP) were measured by NanoDrop. Labeled tumor and reference RNA were mixed and co-hybridized overnight on Agilent custom 44K whole genome microarrays and processed as previously described(6-8). Microarray raw data was uploaded into the UNC Microarray Database(9) where a global LOWESS normalization is performed. The normalized log2 ratios (Cy5/Cy3) of probes mapping to the same gene (Entrez ID as defined by the manufacturer) were collapsed to the average expression value to generate independent gene expression estimates.

Single-cell tumor suspension

First, PDX-tumors were harvested and mechanically digested in a 60 mm dish, using dissection scissors and forceps to mince the freshly isolated tumor into a homogeneous paste. Second, the paste was enzymatically processed using the Miltenyi (Bergisch Gladbach, Germany) human tumor dissociation kit (130-095-929) and this mixture was subjected to gentle rotation for 2 hours at 37°C to obtain a single cell suspension. After incubation, cells were washed twice with 5ml of Hanks'Balanced Salt Solution (HBSS, #14025092) from GIBCO-ThermoFisher Scientific

(Hampton, NH) with 2% of FBS and 10mM HEPES (HF) and then centrifuged at 1,200rpm for 5 min. Cells were resuspended in 1ml of HF and 4mL of Ammonium Chloride Solution (ratio 1:4) (# 07850) from STEMCELL Technologies (Vancouver, Canada) to remove red blood cells and incubated 1-2 min at room temperature. Next, cells were washed with HF and tripsinized in 2 ml of warm 0.05% Trypsin+EDTA (#25300054-GIBCO-ThermoFisher Scientific,Hampton, NH) adding 200 µL of 1 mg/mL DNase I (#07900-STEMCELL Technologies,Vancouver, Canada) for 2 min. The pellet was washed twice in 10mL HF buffer and filtered through a 100µm cell strainer and a 40µm cell strainer, consecutively 1-2 times adding 200 µL of 1 mg/mL DNase I. Finally, cells were counted using trypan blue stain and countess cell counter (Invitrogen Countess Automated Cell Counter C10281 12v) to get a final concentration of ~1000 cells/µl and resuspended in DMEM-F12 (#11320033-GIBCO-ThermoFisher Scientific,Hampton, NH) 2% of FBS.

Single-cell library construction and sequencing

The cell suspensions were loaded on a 10x Genomics Chromium instrument to generate single-cell gel beads in emulsion (GEMs) for targeted retrieval of approximately 10000 cells. Single-cell RNA-Seq libraries were prepared using the following Single Cell 3' Reagent Kits v3: Chromium™ Single Cell 3' Library & Gel Bead Kit v3, PN-1000092; Single Cell 3' Chip B Kit PN-1000074 and i7 Multiplex Kit PN-120262 (10x Genomics, Pleasanton, CA) and following the Single Cell 3' Reagent Kits v3 User Guide (CG000183_ChromiumSingleCell3'_v3_UG_RevB). Libraries were run on an Illumina HiSeq 4000 as 2 × 150 paired end reads. The Cell Ranger Single Cell Software Suite, version 3.1.0 was used to perform sample de-multiplexing, barcode and UMI processing, and single-cell 3' gene counting. A detailed description of the pipeline and specific instructions to run it can be found at: https://support.10xgenomics.com/single-cell-gene-expression/software/pipelines/latest/installation. All generated fastqs were aligned to a combined human (GRCh38) and mouse (mm10) genome references contained within the Cell Ranger software. All 10x single cell RNAseq fastqs and cell ranger output files are available at GEO database (GSE145326).

Each individual experiment scRNAseq cell ranger derived output gene-barcode matrices were analyzed using Seurat R package v.3.0 (10). Individual datasets first underwent a stringent filtering criterion to construct a matrix with relevant genes and cells. For a gene to be selected for downstream analysis, it had to be present in a minimum of three cells in the dataset. Similarly, for a cell to be selected, it had to have a minimum of 1000 uniquely mapped genes. In addition, dead cells and cell doublets were regressed out by calculating metrics like mito.percentage (mito genes/nUMI) and unique genes mapped ratios (nGene/nUMI). The mito percentage was calculated first for human mitochondrial genes and then subsequently for mouse mitochondrial genes. These were different for each individual scRNAseq dataset usually with the upper limit of mito.percentage ranging from 10 for mouse and 20 for human. The unique genes ranged from 6000(mouse)-8000(human) genes per individual dataset. After these filtering steps, the dataset was 'log normalized' by the *Seurat::NormalizeData()* function and scaled using the top 3000 most variable genes by the *Seurat::ScaleData()* function. Further cell subpopulations were identified by calculating the principal components (PC) and utilizing the first 20 PCs by the *Seurat::RunPCA()* and *Seurat::FindNeighbors()* functions respectively. Final cell subpopulation clusters were identified by the *Seurat::FindClusters()* using a resolution of 0.4 and visualized by UMAP plots. Differential expressed (DE) genes were calculated using Wilcoxon rank sum test and the top 100 DE genes were calculated for individual cell subpopulations.

After analyzing each individual dataset in the above manner, we sought to combine all the cells together for a combinatorial analysis. Prior to combination, an additional pre-processing step was performed which was automated doublet/multiplet removal utilizing the DoubletDecon R package(11). Doublets were analyzed using both human and mouse genomes to consider multiples formed within and cross species in our PDX experiment settings. After doublet removal, all the resulting cells were combined into one single cell dataset. This resulted in cell clusters that were separated according to the species and not according to the original experiment. All clusters containing mouse cells, defined by high expression of mouse genes, were removed from further analysis. In this way, combined cell clusters only composed of human cells from all individual experiments was used for downstream analysis (30058 cells in total, 9298 cells from the WHIM11 untreated group, 9777 cells from the BLU9931 treated group and 10983 cells from the treated but released of drug group). We also noted that due to our

scRNAseq mapping process, that very few if any, mouse mRNAseq reads were erroneously mapped into the "human mRNA category" as we previously demonstrated in (12). As the human cells are more homogenous than a mixture of mouse and human cells, we increased the number of variable genes in our next analysis and calculated the top 5000 most variable genes with *Seurat::FindNeighbors()* function. In addition we utilized all the genes and performed scaling for all the genes using the *Seurat::ScaleData()* function. Further cell subpopulations were identified by calculating the principal components (PC) and utilizing the first 30 PCs by the *Seurat::RunPCA()* and *Seurat::FindNeighbors()* functions respectively. Final cell subpopulation clusters were identified by the *Seurat::FindClusters()* using a resolution of 0.2 and visualized by UMAP plots. Resulting Seurat object was used for downstream quantitative cell subpopulation, qualitative DE gene and single cell gene signature analysis. For quantitative cell subpopulation analysis, the number of cells within a cluster was divided between the 3 broad experiment groups (Untreated, Treated and Treated/Released). Qualitative DE gene analysis was performed utilizing Wilcoxon rank sum test by the *Seurat:: FindAllMarkers()* function with the *min.pct* setting at 0.25 and *logfc.threshold* at 0.25. Gene ontology (GO) analysis was performed using the 100 DE genes per cluster (Gene ontology and Gene set analysis methods section). Qualitative gene signature analysis was calculated as average expression of genes defining a particular signature per individual cell in the scale data space. LTS was also calculated per individual cell using the scale data space and the details of this method are expanded in the "Luminal tumor score" method section. All significant genes and gene signatures were visualized as UMAP plots split across the broad experiment groups.

RNA sequencing analysis

Sample Acquisition Clinical Data and Biospecimen Processing

The 206 primary and metastatic tissues were collected from independent sources: GEICAM/2009-03 ConvertHER trial(13) and Hospital Clinic of Barcelona and processed as previously described(14). RNA was quantified using a NanoDrop® Spectrophotometer, and the quality of RNA was then analyzed via 2100 Bioanalyzer Instrument, which using the RNA 6000 Nano assay (Agilent Technologies, Santa Clara, CA) for determination of an RNA Integrity Number (RIN), and only the cases with RIN > 7.0 were included in this study.

RNA sequencing and expression quantification

Gene expression profiles from primary and metastatic tumors were generated by mRNA-sequencing using an Illumina HiSeq 2000 (15). Briefly, 1 μg of total RNA was converted to RNAseq libraries using the TruSeq Stranded Total RNA Library Prep Kit with Ribo-Zero Gold (Illumina, San Diego, CA) and sequenced on an Illumina HiSeq 2000 using a 2x50bp configuration with an average of 136 million read pairs per sample. Quality-control-passed reads were aligned to the human reference CGRh38/hg38 genome using STAR(16). The alignment profile was determined by Picard Tools v1.64 (http://broadinstitute.github.io/picard/). Transcript abundance estimates for each sample were performed using Salmon(17), an expectation-maximization algorithm using the UCSC gene definitions. Raw read counts for all RNAseq samples were normalized to a fixed upper quartile(18). RNAseq normalized gene counts from primary and metastatic tumors were log2 transformed and genes were filtered for those expressed in 70% of samples using the cluster 3.0 software(19). Sequencing data of 166 samples were deposited in the NCBI's genotypes and phenotypes database (dbGaP) (accession number phs001866) and the processed data in GEO (GSE147322). The 40 remaining samples are maintained at the Department of Genetics in the University of North Carolina (UNC) and will be shared upon request.

Supervised analysis of gene expression data

Microarray log2 transformed gene expression data from PDX treated and untreated tumors were filtered for those genes present in 70% of samples and median centered using the cluster 3.0 software(19). Missing data was imputed using Euclidean distance to find the nearest neighbor and calculate the missing value using the impute.knn R function(20). To identify significant gene expression changes in treated PDX WHIM11 tumors with BLU9931 compared with the untreated we used two-class Significance Analysis of Microarrays (SAM)(4, 5) using 'samr' package in R. Hierarchical clustering of resulting gene lists was performed with Cluster 3.0(19) across 1198 breast tumors and normal samples from TCGA dataset. Clustering results were viewed with Java Treeview version 1.1.6r4 (21, 22). Additional signatures were identified by selecting correlating gene nodes (r= > 0.5).

To identify significant gene expression changes in MIB-captured kinases in treated PDX WHIM11 tumors with BLU9931 compared with the untreated group or the released group, we used two-class Significance Analysis of Microarrays (SAM)(4, 5) using 'samr' package in R. Hierarchical clustering of resulting gene lists was performed with Cluster 3.0(19)
For RNAseq data, samples were normalized and log2 transformed from 170 primary tumor-metastasis pairs and divided into two different datasets: (1) 77 luminal pairs (only Luminal A/B and/or HER2 samples in the primary and their counterpart metastatic tumors were selected) and (2) 8 basal pairs. 36 Pairs with PAM50 classification of Normal-like in primary or metastatic tumors were removed from the analysis. Each dataset was median centered separately using the cluster 3.0 software(19). Missing data was imputed using Euclidean distance to find the nearest neighbor and calculate the missing value using the impute.knn R function(20). To identify significantly overexpressed genes in metastatic compared with primary tumors we used two-class paired SAM (4, 5).

PAM50 subtype classification

To avoid confounding effects of the murine host tissue on gene expression patterns of human PDX tumors, we first adjusted PDX data values using a WHIM11-to-TCGA cohort adjustment factor. For this approach, the expression of each gene was calculated by taking the difference in gene summary measures (median) between the untreated WHIM11 tumors and the HER2E TCGA samples (since it has been previously described that WHIM11 is a HER2E tumor(23, 24)); this difference established the adjustment factor to be used for each of the PDX samples. Thus, for each PDX tumor sample, the gene expression estimates were adjusted by subtracting each of the adjustment factors from its corresponding gene measurement. The adjusted microarray data of 13 PDX and TCGA tumors were then subtyped by the 50-gene PAM50 predictor(25). The PAM50 predictor calculates, for each sample, the correlation coefficient to each of the 5 PAM50 centroids (Luminal A, Luminal B, Basal-like, HER2-enriched, and Normal-like). For each BC cell lines, we calculated the Euclidean distance of each cell line to each of the tumor subtype centroids, and assigned a subtype call where the lowest distance was identified(26).

For 154 primary and metastatic tissues all tumors and 855 primary tumors dataset intrinsic molecular subtype of breast cancer were assigned as previously described (14, 27). In addition to the subtype classification, we calculated a PAM50 proliferation score using the previously described 11-gene signature (BIRC5, CCNB1, CDC20, CDCA1, CEP55, KNTC2, MKI67, PTTG1, RRM2, TYMS, UBE2C)(25).

Luminal tumor score

Previous work has demonstrated the broad explanatory power of leveraging a transcriptome wide model of normal epithelial cell differentiation(28). Here we use the same computational framework to model the variation among luminal tumor cell states. The model is supervised using the well characterized TCGA cohort. Upper quartile normalized gene counts were retrieved from Firehose (http://gdac.broadinstitute.org/runs/stddata__2016_01_28/data/BRCA/20160128/gdac.broadinstitute.org_BRCA.Merge_rnaseqv2__illuminahiseq_rnaseqv2__unc_edu__Level_3__RSEM_genes_normalized__data.Level_3.2016012800.0.0.tar.gz) then log transformed and median centered. Distance weighted discrimination (DWD) was performed to identify the optimal axis of segregation between HER2E and Luminal A tumors using TCGA dataset. Samples were then projected along this HER2E-Luminal A axis to produce a relative score, the 'luminal tumor score' (LTS) for each sample. In other words, each gene expression value was multiplied by the weight of DWD output for each gene and all the resulting values were summed up obtaining a single score per sample.

Gene expression signatures and supervised hierarchical clustering

For each dataset analyzed, the FGFR4 gene signature (FGFR4-induced and FGFR4-repressed signature) was calculated as the average of each gene expression value present in the signature for each sample of the set used. To calculate the significant modules/signatures of each dataset, we applied a collection of 691 gene expression modules, representing multiple biological pathways and cell types, to all primary and metastatic tumors summarized in Supplemental table 6. These signatures were obtained from old 454 publications partially summarized previously (29, 30), 41 Gene set enrichment analysis (GSEA) signatures published in the Molecular Signature Database(31) and newly generated signatures completing 4 different types of

signatures. In summary, (1) 599 modules were calculated as the median of each gene expression value present in the signature for each sample of the set used; (2) 11 modules were used as a single gene expression value; (3) 48 named as special models and calculated as it is been previously described using predefined algorithms(15, 28, 32-51) (in order to implement each modules, the methods detailed in the original studies were followed as closely as possible); (4) 31 signatures were newly built using two distinct hierarchical clustering analysis of the TCGA breast cancer data. We first developed new immune/related gene list from (1) where all the previous immune module gene lists were pooled generating a unique list of 2249 genes; we next used TCGA breast cancer 1198 samples to generate a supervised hierarchical cluster derived from these immune-related gene list and picked individual nodes/clusters with a node correlation>0.5. We obtained 11 clusters associated with immune-cell infiltrates (modules starting with "TCGA.BRCA.1198_immune"). Second, using same TCGA gene expression samples we perform an unsupervised cluster with the top 2000 most variable expressed genes. By selecting nodes with a correlation > 0.5 from the hierarchical clusters, we picked 21 more clusters, and used them as new signatures (modules starting with "TCGA.BRCA 1198_") (Supplemental table 6).

Once we calculated the gene signature score for each module we performed SAM analysis between metastatic and primary tumors to identify significantly changed modules. Results were hierarchically clustered with Cluster 3.0(19) and viewed with Java Treeview version 1.1.6r4 (21, 22). Finally, the cluster-derived signatures were obtained by selecting nodes with a correlation > 0.5 from the supervised hierarchical cluster. Some gene signatures were box plotted according to primary and metastatic signature score using Graphpad Prism software.

Gene ontology and Gene set analysis

To measure gene sets significantly associated with a phenotype of interest the Broad Institute makes available several gene set collections or MSigDB(52). We have used the collection gene ontology (GO) gene sets or collection 5 (curated sets derived by gene ontology) available in (http://www.broadinstitute.org/gsea/msigdb/index.jsp) to associate our gene cluster of interest (microarrays, or scRNAseq) with the biological process, molecular function and cellular component of the cells(53) (Supplemental Table 2).

To measure the association between a biological state or process and the gene expression profile we used gene set enrichment analysis (GSEA) (version 3.0) [http://www.broadinstitute.org/gsea/] with 1000 permutations and refined Hallmark collection(31) as defined gene set (Supplemental Table 3).

Mutation calling from FFPE RNA-seq

Paired-end FASTQ files were aligned to the reference genome CGRh38/hg38 vd1 (GRCh38.d1.vd1.fa) from Genomic Data Commons (GDC) (https://gdc.cancer.gov/about-data/data-harmonization-and-generation/gdc-reference-files). RNA-Seq alignments and transcript abundance estimates for each sample were performed using STAR(16)/Salmon(17) workflow (v2.4.2a)(https://github.com/alexdobin/STAR). Next, we used Strelka2(54, 55) (version 2.9.2) in germline RNA mode reporting the small variant predictions in VCF format(56).Variant calls were annotated using variant effect predictor (VEP)(57) tool. We used various filters to ensure high confidence mutation calls. We only included mutations described in the COSMIC mutation data database(58, 59), mutations with a total coverage of 10 reads, a mutant allele frequency >0.25, and only included mutations with a variant allele frequency <0.01 for the population maximum reported in the genome aggregation database (gnomAD)(60, 61). Intron variants and synonymous variants were not considered in this analysis.

WES and mutation detection

For whole exome sequencing of WHIM11 PDX tumor, genomic DNA was isolated using a QIAGEN (Hilden, Germany) AllPrep DNA/RNA Mini Kit (#80204). DNA libraries were selected and amplified using the Sure Select Target Enrichment for Illumina paired-end Multiplexed sequencing Library kit. Final library size selection used approximately 300 bp fragments with a final concentration of 10ng/ul. Quality of libraries and captured exomes were measured using the Agilent Technologies (Santa Clara, CA) Tapestation DNA 1000 and High Sensitivity D1000. Paired end (2 x100 bp) sequencing was done using Illumina Nextseq 500 at the UNC Translational Genomics Lab (TGL). Reads were aligned to human genome hg38 (GRCh38.d1.vd1) using BWA-MEM(62). Biobambam was used to mark duplicates (63). Allele counts at loci of interest were calculated using a simple pileup counter. We analyzed the 31 mutations described in WHIM11 in Shunqiang Li et. al(23). Next, we calculated the proportion

of sequencing reads that contained a mutant allele. This value was expressed as a percentage (variant allele frequency [VAF]). The VAF is determined by counting how many times the altered allele appears in the population then dividing by the total number of copies of the gene (altered allele plus reference allele).

Patients, samples and clinical data

The Cancer Genome Atlas (TCGA) were collected as previously described(64, 65). In total 1100 tumors and 98 matched normal tissue were assayed by RNA sequencing, SNP-based copy number analysis and somatic mutations all collected from (https://doi.org/10.7908/C11G0KM9)(15, 64, 66). From 1198 samples, normal-like patients and true-normal tissues have been removed from the analysis.

Molecular Taxonomy of Breast Cancer International Consortium (METABRIC) was collected as previously described(67) and the data was obtained from the European Genome-Phenome Archive (accession number: EGAS00000000083)(67) and clinical information from(68). For survival analysis, patients with normal-like tumors or those lacking informative censoring were excluded to establish a 1672 sample dataset. The 855 human breast tumor gene expression microarrays taken from the public domain and previously published by Harrell, et. al(69). Microarray data previously published by the MDACC group(70) was obtained under the GEO accession number (GSE25066). For survival analysis patients without informative censoring and normal-like have been excluded from the analysis remaining 447 samples. PDX mRNA-seq data was obtained from(23, 24) and is deposited with dbGAP under accession number phs000611 (http://www.ncbi.nlm.nih.gov/projects/gap/cgi-bin/study.cgi?study_id=phs000611.v1.p1) All tumors were assigned to an intrinsic molecular breast cancer (Luminal A, Luminal B, HER2E, Basal and Claudin-low), using the PAM50 classifier(25, 71) or Claudin-low predictor(28) from each original published dataset.

Cell line data for obtaining Genetic Dependency Combined RNAi (Broad, Novartis, Marcotte) scores (DEMETER2) and Gene expression Public 19Q1 (RNAseq gene expression data (log2(TPM+1)) was downloaded from Cancer Dependency Portal (DepMap) (https://depmap.org/portal/download/).

Statistics

Mann-Whitney tests (two-tailed), one-way ANOVA, and paired *t*-tests were performed with GraphPad Prism® 6.0 software and/or RStudio version 1.1.383 (http://cran.r-project.org). Overall survival was defined as the period of time to death or last follow-up. Estimates of survival were from the Kaplan–Meier curves and tests of differences by the log-rank test and univariate Cox models. Multivariate Cox models were used to test the independent prognostic significance of each variable. Linear correlation between two variables was measured as the Pearson correlation coefficient and calculated in RStudio version 1.1.383 (http://cran.r-project.org). All statistical tests were two sided, and the statistical significance level was set to less than 0.05 unless specified otherwise.

2. Supplemental Figures 1-13

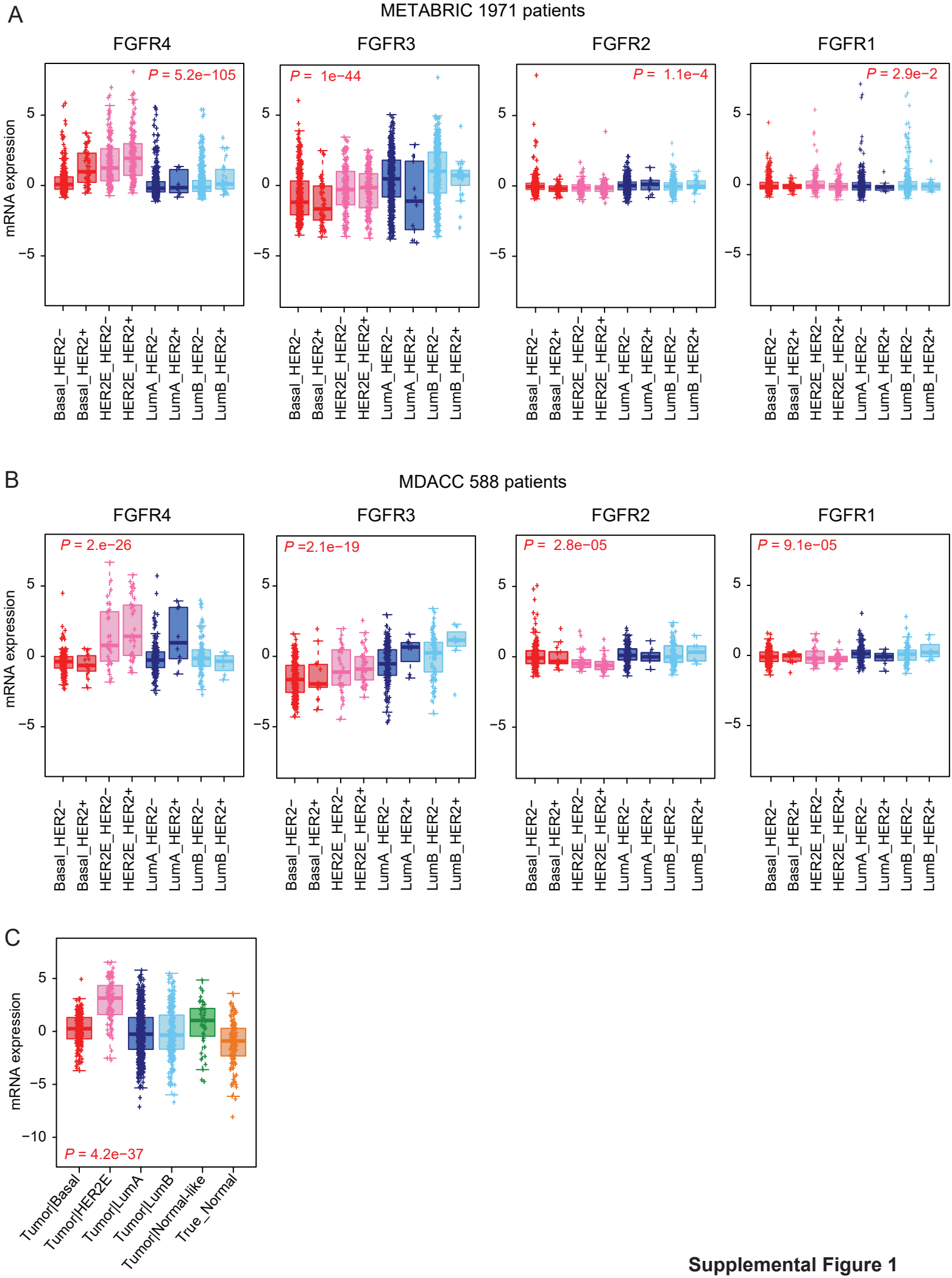

Supplemental Figure 1

Supplemental Figure 1. Comparative genetic and transcriptomic analysis of FGFR4 family members in METABRIC and MDACC datasets. A, B, Boxplot of FGFR family gene expression levels by mRNAseq (METABRIC, 1971 patients) and microarrays (MDACC, 588 patients) gene expression data according to molecular subtype and HER2 status by IHC. Tumors without clinical data for HER2 status and Normal-like samples have been removed from the remaining analysis. **C**, Boxplot of FGFR4 gene expression levels by mRNAseq in TCGA breast tumors compared with normal breast tissue. Boxplot displays the median value on each bar, showing the lower and upper quartile range of the data and data outliers. The whiskers represent the interquartile range. Comparison between more than 2 groups was performed by ANOVA. Statistically significant values are highlighted in red. Each mark represents the value of a single sample.Each mark represents the value of a single sample. LumA: Luminal A, LumB: Luminal B, HER2+: HER2 positive, HER2-: HER2 negative.

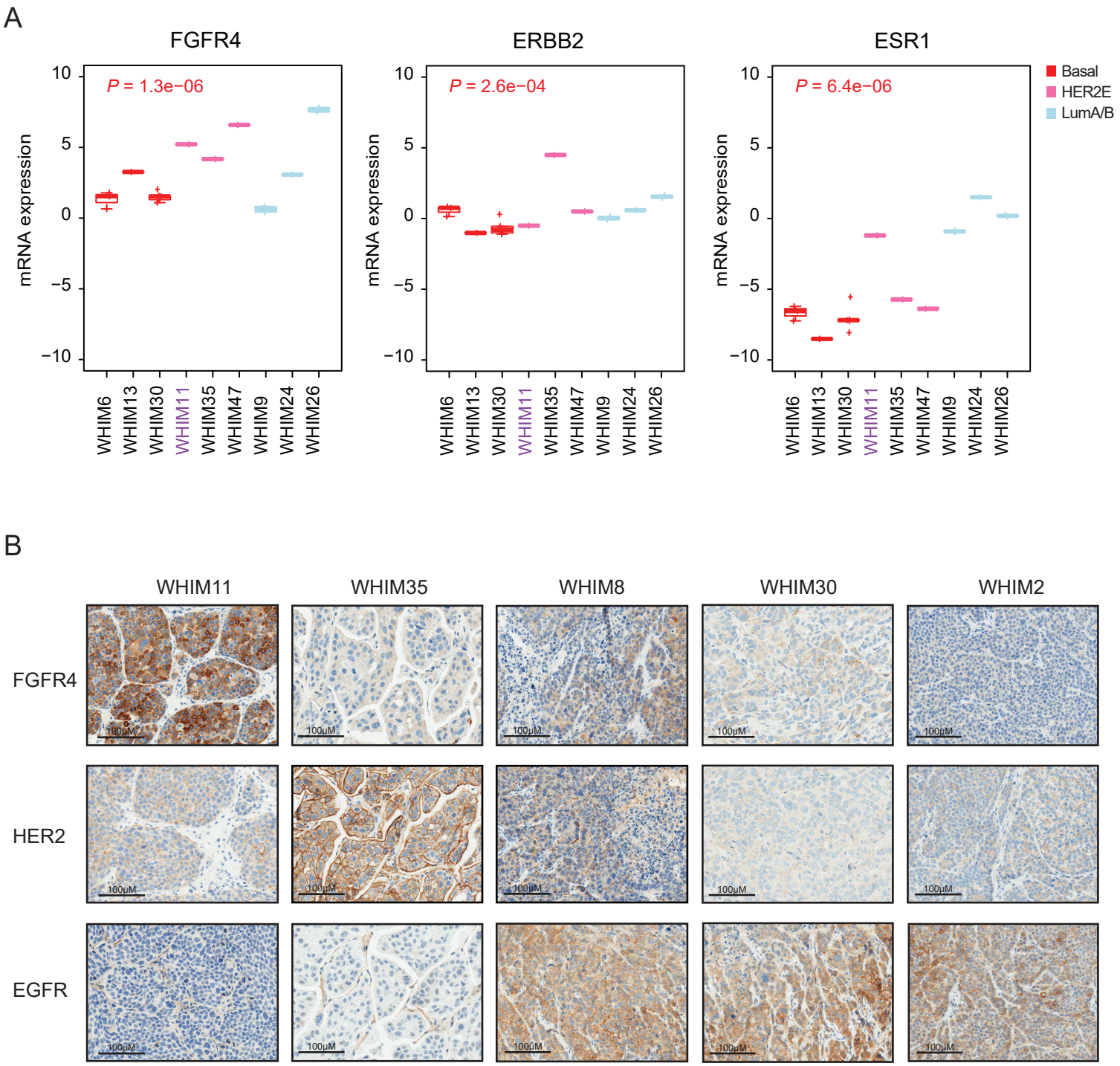

Supplemental Figure 2

Supplemental Figure 2. Genomic biomarkers of WHIMs models. A, Comparative mRNA expression of FGFR4, ERBB2 and ESR1 mRNA of 3 representatives Basal (WHIM6 (n=3), WHIM13(n=1), WHIM30(n=5), HER2E (WHIM11(n=1), WHIM35(n=1), WHIM47(n=1) and Luminal (WHIM9(n=2), WHIM24(n=1), WHIM26(n=2)) WHIM models. WHIM11 is highlighted in purple color. Comparison between groups was performed by ANOVA. **B**, IHC staining for FGFR4, HER2 and EGFR in WHIM11, WHIM35, WHIM8, WHIM30 and WHIM2 untreated tumors. Scale bar 100 µM. Nuclear staining: Haematoxylin.

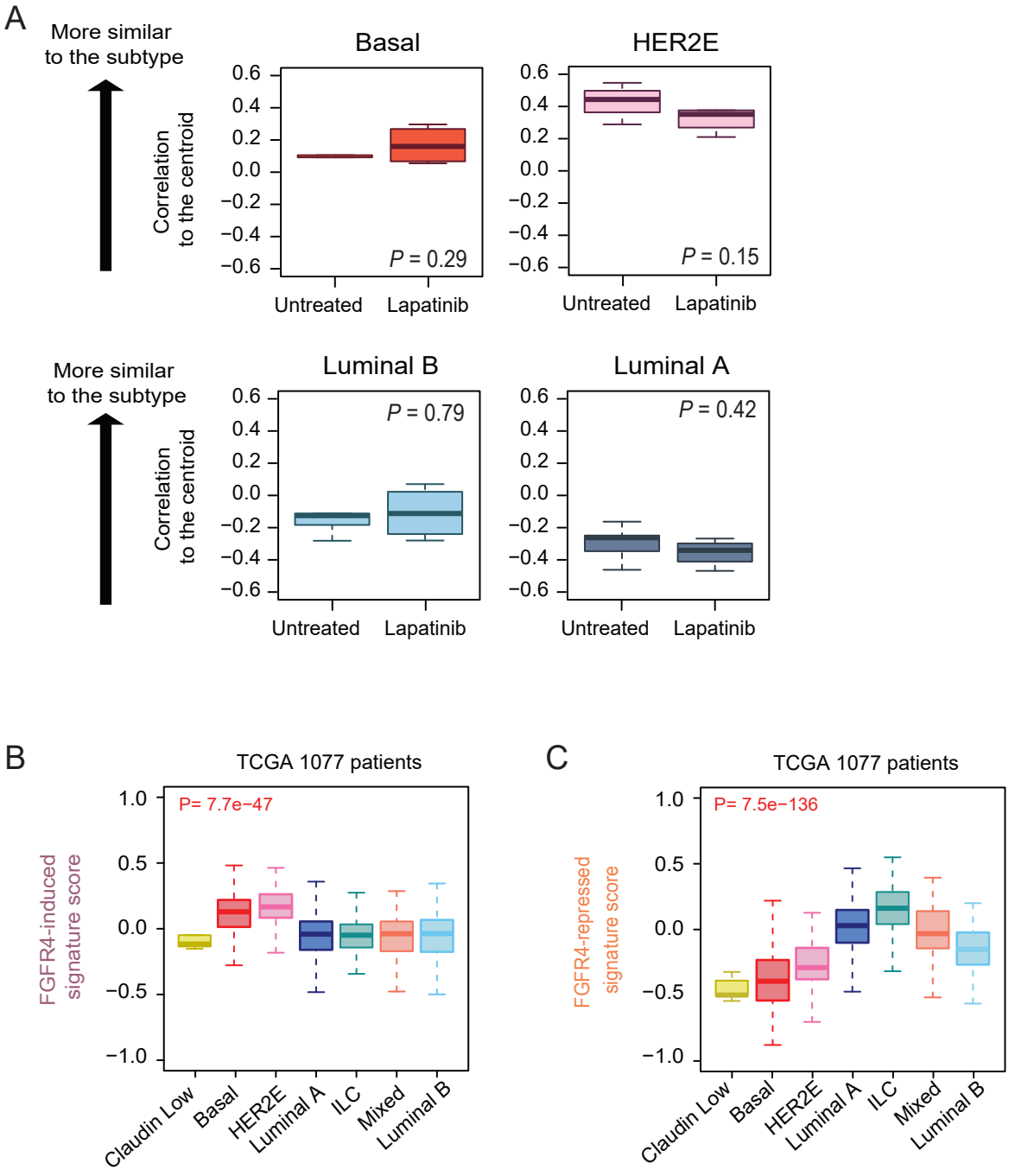

Supplemental Figure 3

Supplemental Figure 3. A, Correlation to the PAM50 centroids (Basal, HER2E, Luminal A and Luminal B) of Lapatinib treated and untreated mice. Comparisons between two paired groups were performed by paired t-test (two-tailed). **B**, Expression levels of FGFR4-induced and repressed (**C**) signatures in TCGA dataset tumors divided by the histologic subtypes and molecular intrinsic subtypes. From 1198 samples, normal-like patients and true-normal tissues have been removed from the analysis. In addition ILC and mixed are shown as separate groups. Statistical differences are calculated by ANOVA test. Most of the tumors were Invasive ductal carcinoma (IDC) except: ILC: Invasive lobular carcinoma and Mixed ILC+IDC. Boxplot displays the median value on each bar, showing the lower and upper quartile range of the data. The whiskers represent the interquartile range. Statistically significant values are highlighted in red.

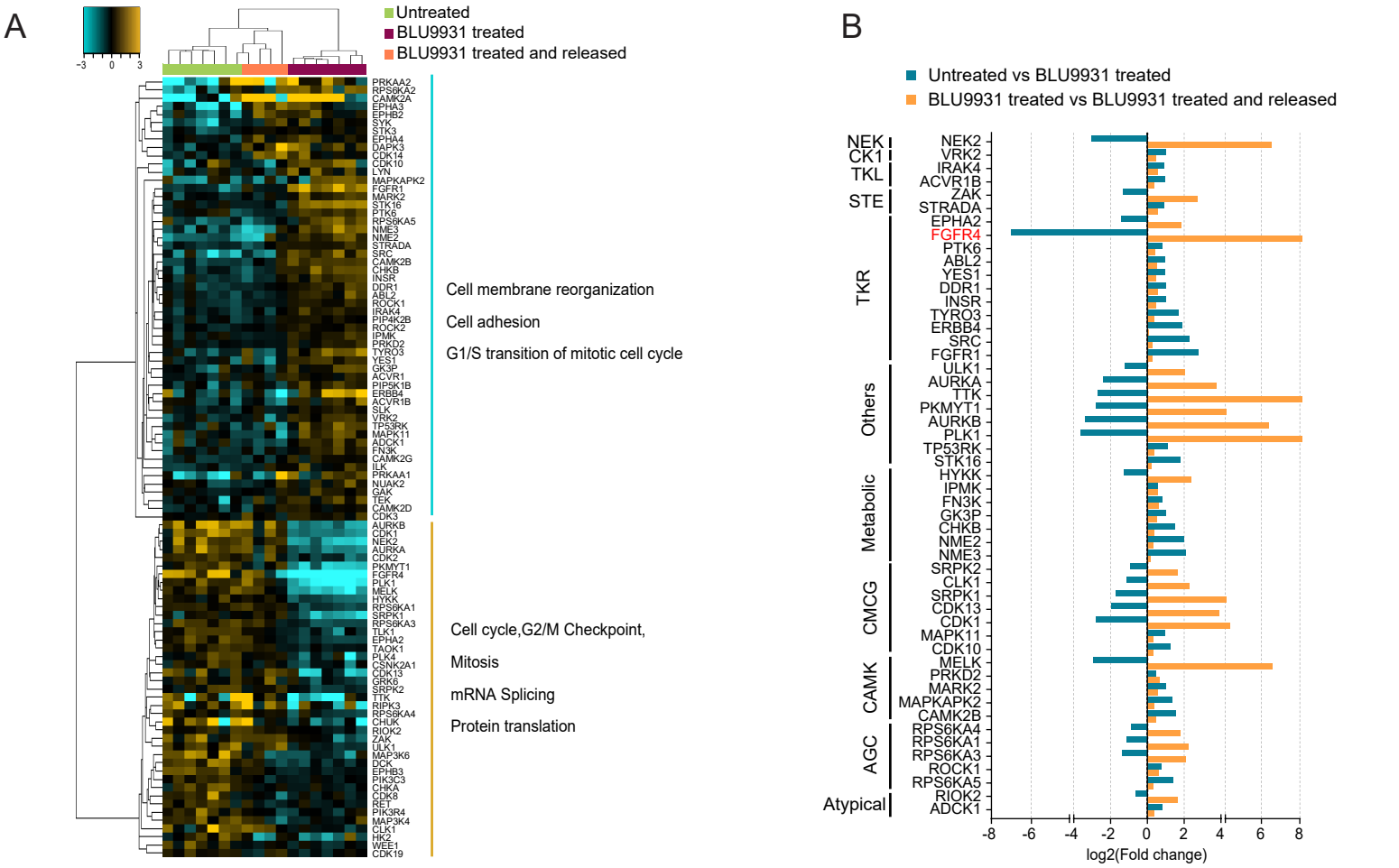

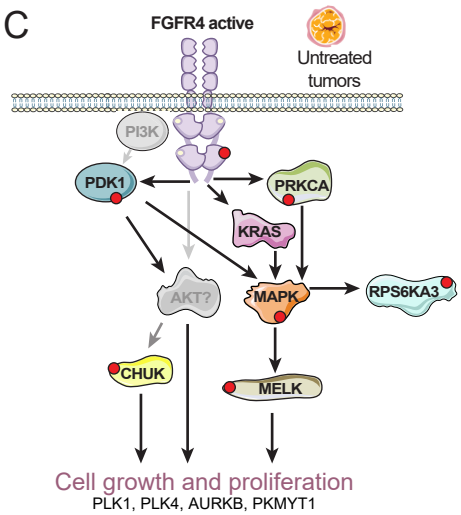

Supplemental Figure 4

Supplemental Figure 4. A, Supervised analysis of the quantified kinases significantly altered and GO annotations for each cluster after treating WHIM11 tumor (0.6g/Kg/day) for 18 days in the untreated (n=7), BLU9931 treated (n=4) and BU9931 treated but drug released group (n=7). **B,** 95 commonly differentially altered kinases found between the untreated and the BLU9931 treated but drug released group. Bar plot shows only the log2-Fold Change LFQ values of the significant kinases (FDR 5%) divided by kinases family groups. **C**, Schematic pathway of FGFR4 signaling where the colored proteins are the significant altered genes, the red dots correspond to the common significant altered kinases and in grey the predicted upstream regulator genes. NEK: NIMA-related protein kinase family, CK1: Casein kinase 1 family, TKL: Tyrosine Kinase-Like group, STE: Serine/threonine kinases, TKR: Tyrosine kinase receptor family, Others: Serine/Threonine-related kinases, CMCG: including cyclin-dependent kinases (CDKs), mitogen-activated protein kinases (MAP kinases), glycogen synthase kinases (GSK) and CDK-like kinases, CAMK: Ca2+/calmodulin-dependent protein kinase, AGC: 63 evolutionarily related serine/threonine protein kinases. This figure was made using Servier Medical Art collection (http://creativecommons.org/licenses/by/3.0).

A

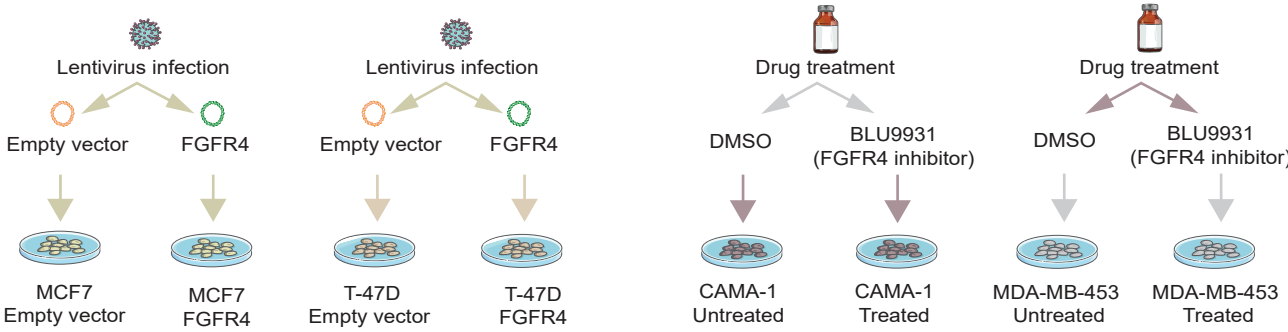

B

	MCF7	T-47D	CAMA-1	MDA-MB-453
Control	MCF7-Empty vector	T47D-Empty vector	CAMA-1 treated	MDA-MB-453 treated
FGFR4 Active	MCF7-FGFR4	T47D-FGFR4	CAMA-1 Untreated	MDA-MB-453 Untreated

Supplemental Figure 5

Supplemental Figure 5. A, Schematic outline showing the in vitro experimental design used with 4 different BC cell lines (MCF-7, T-47D, MDA-MB-453 and CAMA-1). Both, MCF7 and T-47D BC cells were infected with pLOCTurbo-RFP (named Empty vector), and pLOC-FGFR4 (named FGFR4) derived lentiviral vector. MDA-MB-453 and CAMA-1 were treated with BLU9931 (FGFR4 inhibitor) at 2.5 and 10 μM, respectively for 48 hours. B, Schematic used to calculate the Euclidean distance and LTS (at least 4 replicates in each cell line). The control group contains four cell lines with a low FGFR4 activity (either due to low expression or by targeted pathway inhibition). The FGFR4 active contains four cell lines with a higher FGFR4 expression/activation.

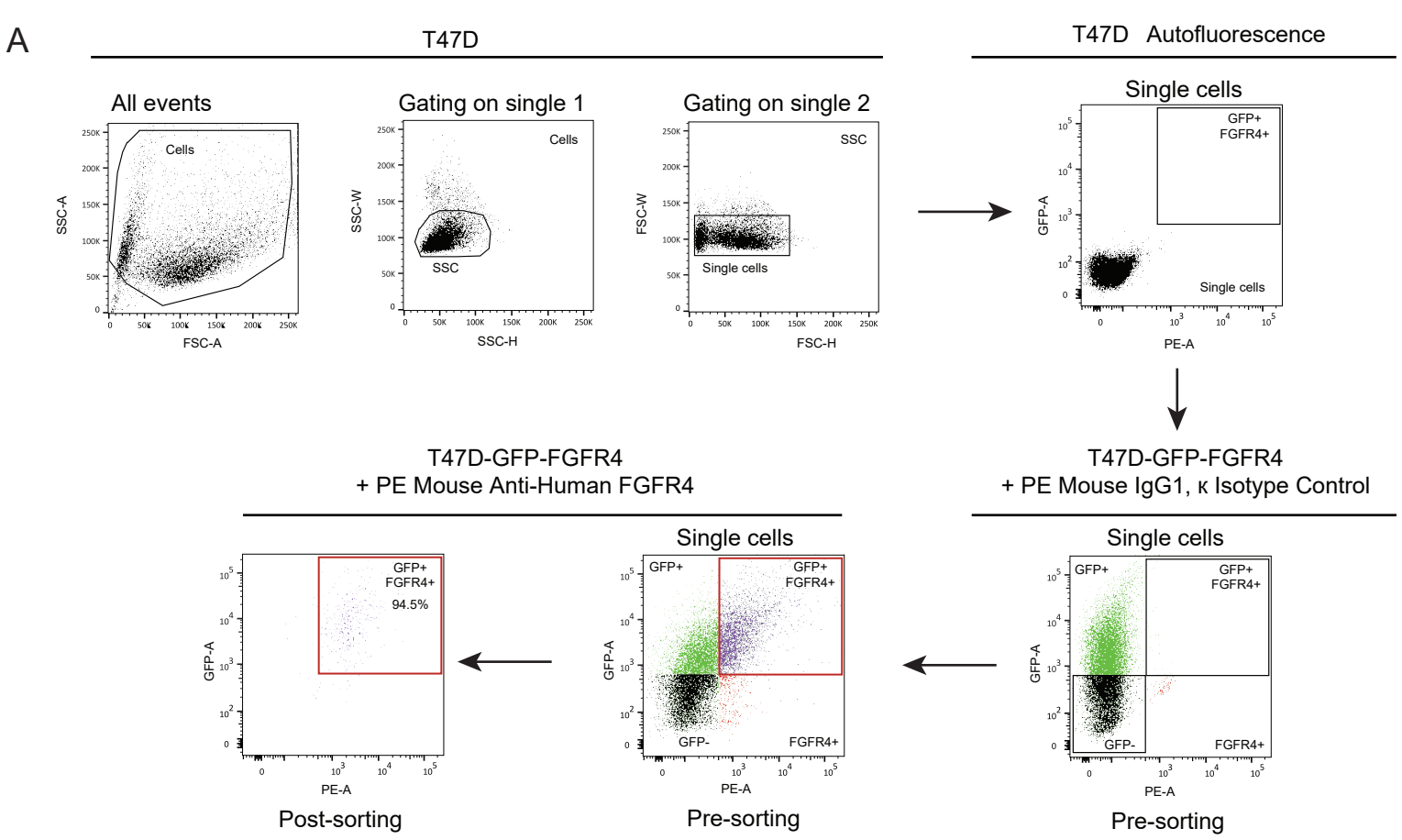

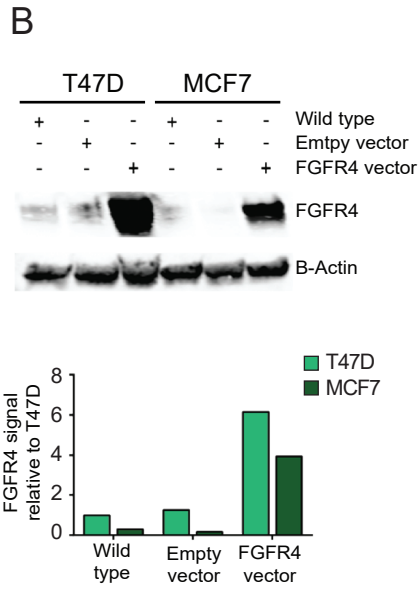

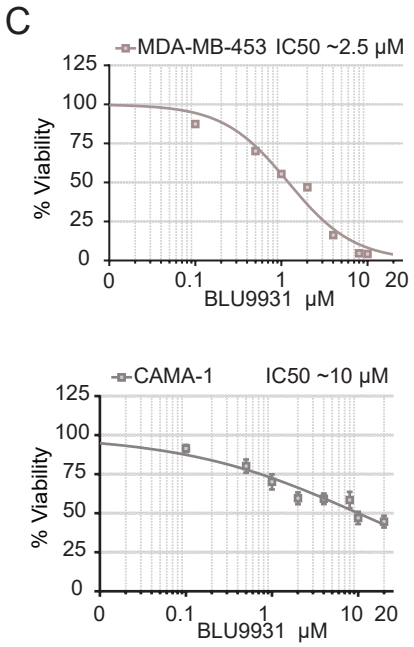

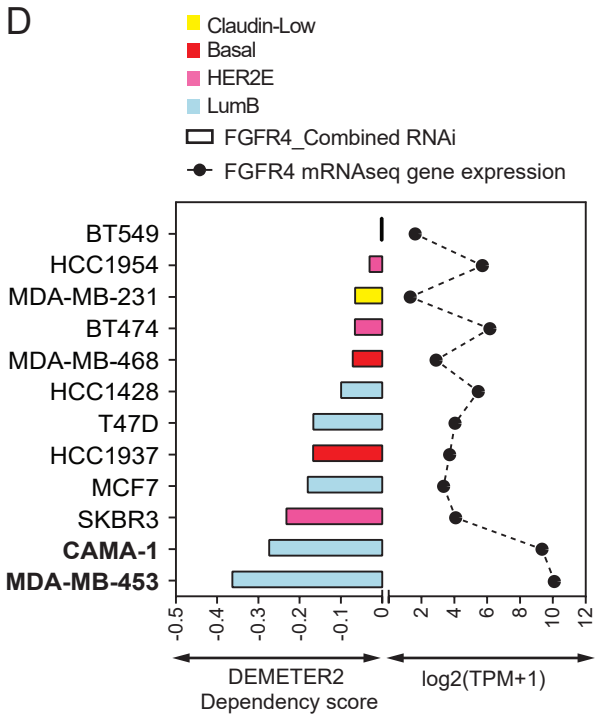

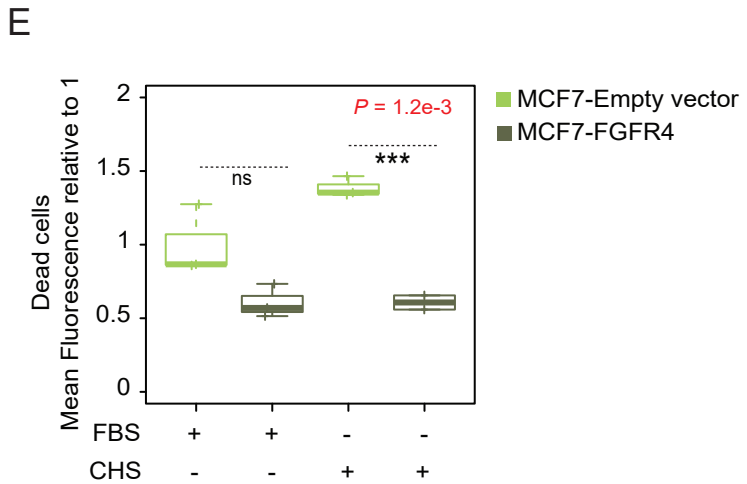

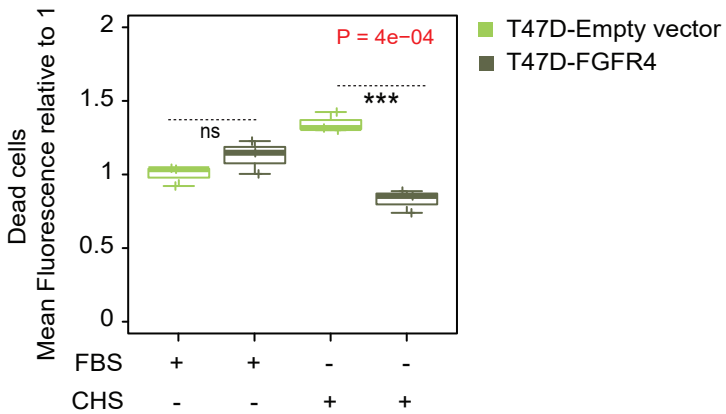

Supplemental Figure 6

Supplemental Figure 6. A, Representative strategy of cell selection by FACS of T47D-GFP-FGFR4 positive cells (same strategy was used with the controls (empty vector) and MCF7 cell line). Cells were first selected according to their morphology and the doublets were excluded. Sorting gates were determined using MCF7-GFP-FGFR4 labeled with a PE Mouse IgG1, κ Isotype as a control of GFP+/PE negative cell population and a PE-mouse anti-human FGFR4 antibody to select GFP+/FGFR4-PE+ cells. The percentages of total cells after sorting is represented within the gates. **B**, Western blot and fluorescent quantification of FGFR4 protein on MCF7 and T47D empty vector or FGFR4 overexpressing engineered cells. **C**, MTT cell growth assay measurements of half-maximal inhibitory concentration (IC50) of BLU9931 in MDA-MB-453 and CAMA-1 cell lines for 48h. **D**, DEMETER2 (dependency score) compared with FGFR4 RNAseq gene expression data (log2(TPM+1)) in a panel of breast cancer cell lines. A lower DEMETER2 score implies that a gene is more likely to be essential in a given cell line. A score of 0 is equivalent to a gene that is not essential. Higher log2(TPM+1) scores implies higher gene expression data in a given cell line. **E**, 7-AAD cell viability assay comparing MCF7 or T47D Empty vector and MCF7 or T47D - FGFR4 cells after 6 days of estrogen deprivation using charcoal stripped fetal bovine serum. All quantitative data was generated from three replicates. Mean fluorescence of 7-AAD positive cells was analyzed by cell cytometry and are shown as dead cells. FBS: Fetal bovine serum, CHS: Charcoal stripped fetal bovine serum. Data were compared with ANOVA statistical model. Comparisons between two paired groups were performed by paired t-test (two-tailed). Significant *P* values are indicated as * $P<0.05$, ** $P<0.01$ and *** $P<0.001$ and **** $P<0.0001$. Statistically significant values are highlighted in red. Boxplot displays the median value on each bar, showing the lower and upper quartile range of the data. The whiskers represent the interquartile range.

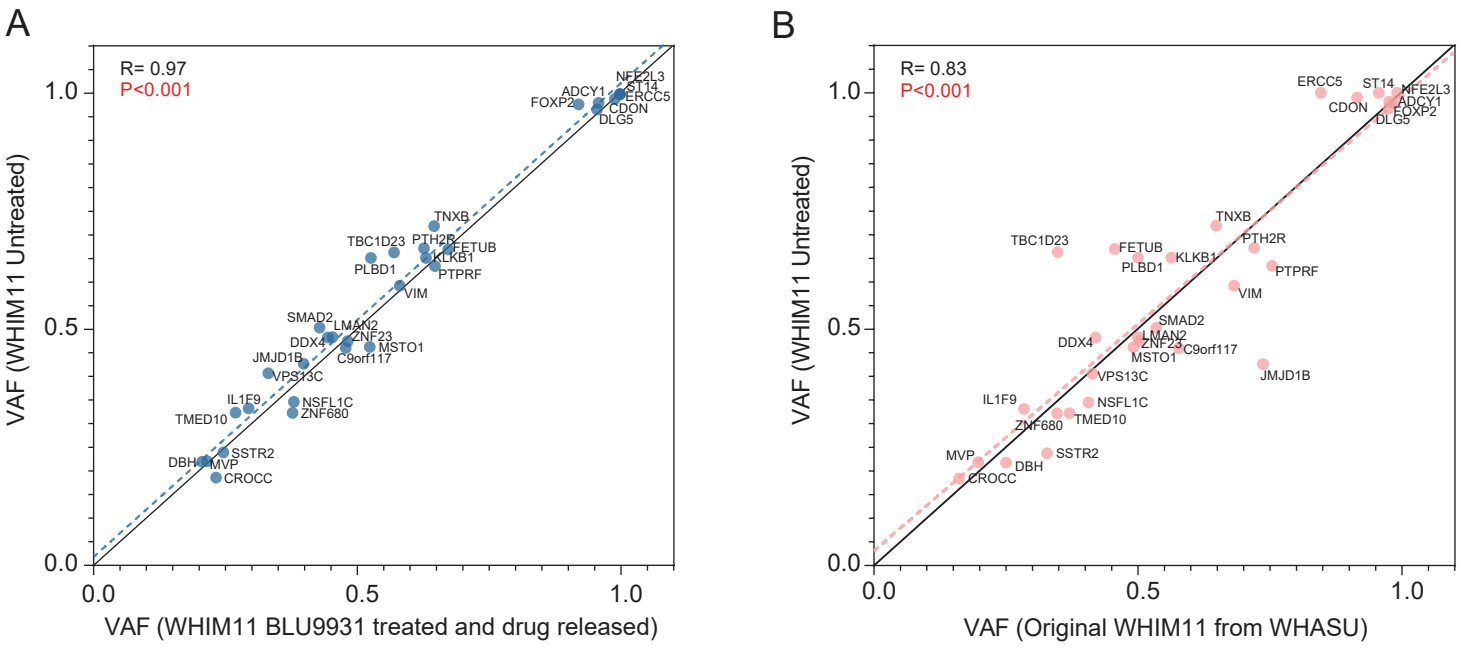

Supplemental Figure 7

Supplemental Figure 7. A, Correlation plots of VAF in 31 genes mutated between WHIM11 untreated tumors (n=2) and WHIM11 BLU9931 treated for 18 days and collected 14 days after drug removal (n=2). **B**, Correlation plot VAF in 31 genes mutated between WHIM11 untreated tumors (n=2) and previously published and original WHIM11 PDX. Correlation was measured using the Pearson correlation coefficient.

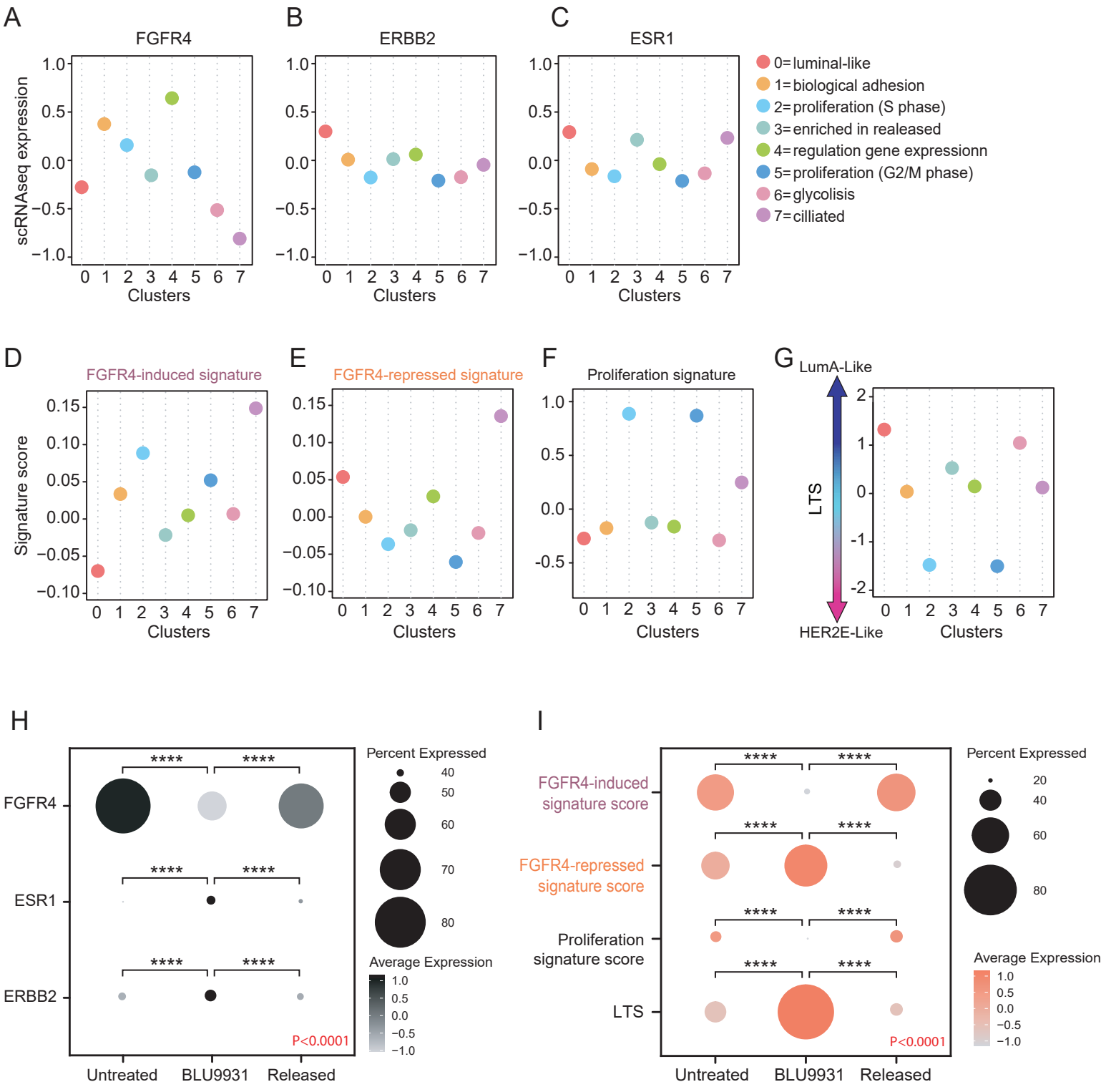

Supplemental Figure 8

Supplemental Figure 8. Dot plots showing the gene expression or gene signature mean of each cluster in the scale data space presented in the UMAP analysis on Figure 4A of FGFR4(**A**), ERBB2(**B**) and ESR1(**C**), FGFR4-induced signature(**D**), FGFR4-repressed signature(**E**), Proliferation signature (**F**) and luminal tumor score(LTS) (**G**). **H,** Dot plot showing the average expression of FGFR4, ERBB2 and ESR1 genes in all cells analyzed of WHIM11 tumor (untreated, n=2) versus WHIM11 BLU9931 treated tumor (BLU9931, n=2) that was allowed to regrow after removal of BLU9931 (Released, n=2). **I,** Dot plot showing the average expression of FGFR4-induced and repressed signature, proliferation signature and LTS of WHIM11 tumor (untreated, n=2) versus WHIM11 BLU9931 treated tumor (BLU9931, n=2) that was allowed to regrow after removal of BLU9931 (Released, n=2). Comparison between groups was performed by ANOVA. Comparisons between two groups was performed by Tukey test (two-tailed). Significant *P* values are indicated as * $P<0.05$, ** $P<0.01$, *** $P<0.001$ and **** $P<0.0001$. For figures A-G, the average expression of either the respective gene or signature is represented as the overall average of its expression in all the cells within that respective cluster. For figures H-I, the average expression of either the respective gene or signature is represented as the overall average of its expression in all the cells within that respective experiment group.

A

LUMINALS IN PRIMARY DATASET

PAM 50	Metastasis				
Primary	Basal	HER2E	LumA	LumB	Pairs
HER2E (11)	2 (16.6%)	8 (66,6%)	1 (8.3%)	0 (0%)	11
LumA (39)	0 (0%)	6 (15%)	18 (45%)	15 (37.5%)	39
LumB (27)	0 (0%)	4 (13.8%)	5 (17.2%)	18 (62.1%)	27
				Total pairs	77

B

BASALS IN PRIMARY DATASET

PAM 50	Metastasis				
Primary	Basal	HER2E	LumA	Lum B	Pairs
Basal (8)	8 (100%)	0	0	0	8
				Total Pairs	8

C

Complete dataset	Metastasis				
Primary	Basal	HER2E	Lum A	Lum B	Pairs
Basal	8 (100%)	0	0	0	8
HER2E	2 (16%)	8 (66.6%)	1 (8.3%)	0	11
Lum A	0	6 (15%)	18 (45%)	15 (37,5%)	39
Lum B	0	4 (13.8%)	5 (17.2%)	18 (62.1%)	27
				Total Pairs	85

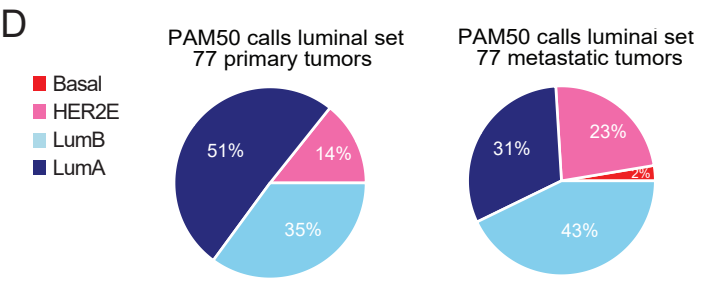

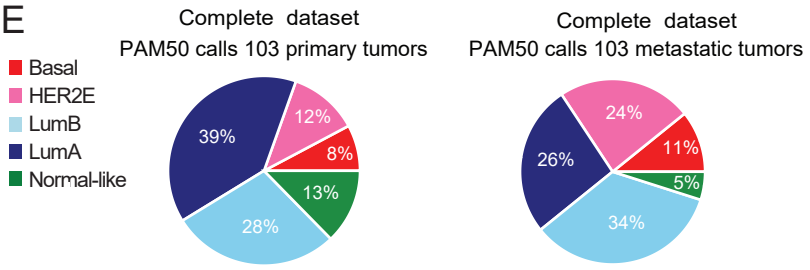

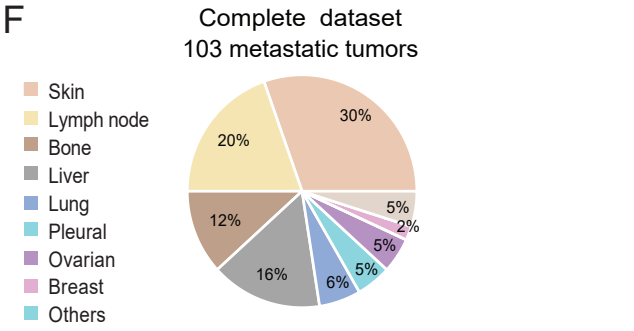

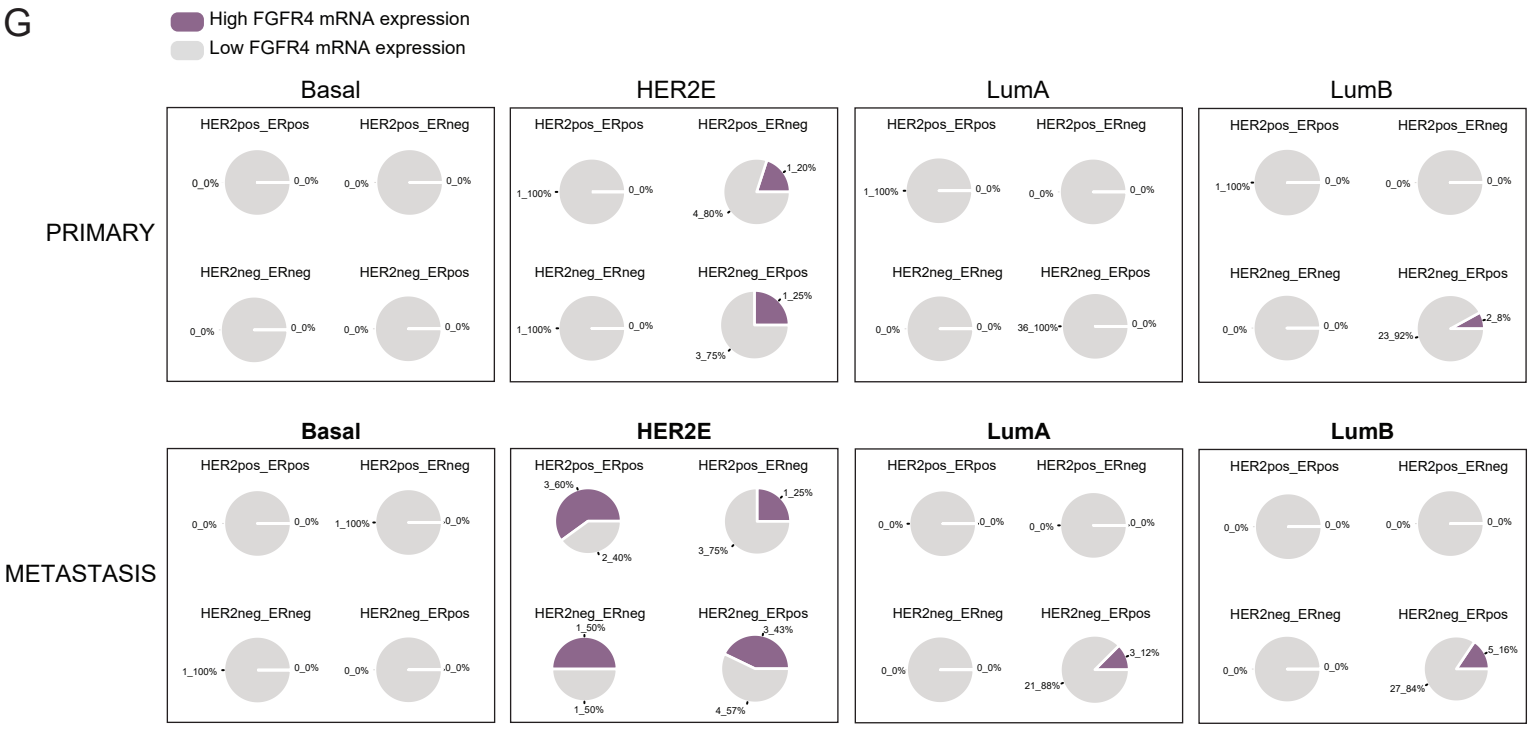

Supplemental Figure 9

Supplemental Figure 9. A, Molecular intrinsic subtype change between primary and metastatic tumors in luminal tumors and **B**, Basal tumors**. C**, Molecular intrinsic subtype change between primary and metastatic tumors in the complete set of 102 paired primary and metastatic tumors without normal-like pairs. Samples (and the pair) called normal-like in either the primary or metastatic tumors were removed from the analysis resulting in 85 pairs. **D**, Molecular intrinsic subtype percentages in primary (left pie chart) and metastatic tumors (right pie chart) of 77 paired samples (luminal dataset). **E**, Molecular intrinsic subtype percentages in primary (left pie chart) and metastatic tumors (right pie chart) of 102-paired samples (204 tumors, entire dataset with intrinsic subtype information). **F,** Distribution of sites of distant metastasis using the complete set (102 metastatic tumors). **G,** Pie charts of FGFR4 high and low expression in the complete set of 102 tumors divided by subtype and by clinical HER2/ER positivity. FGFR4 mRNA expression was considered high expression when is greater than 75% of positive values in RNAseq median centered data. LumA: Luminal A, LumB: Luminal B. HER2pos: HER2 positive, HER2neg: HER2 negative.

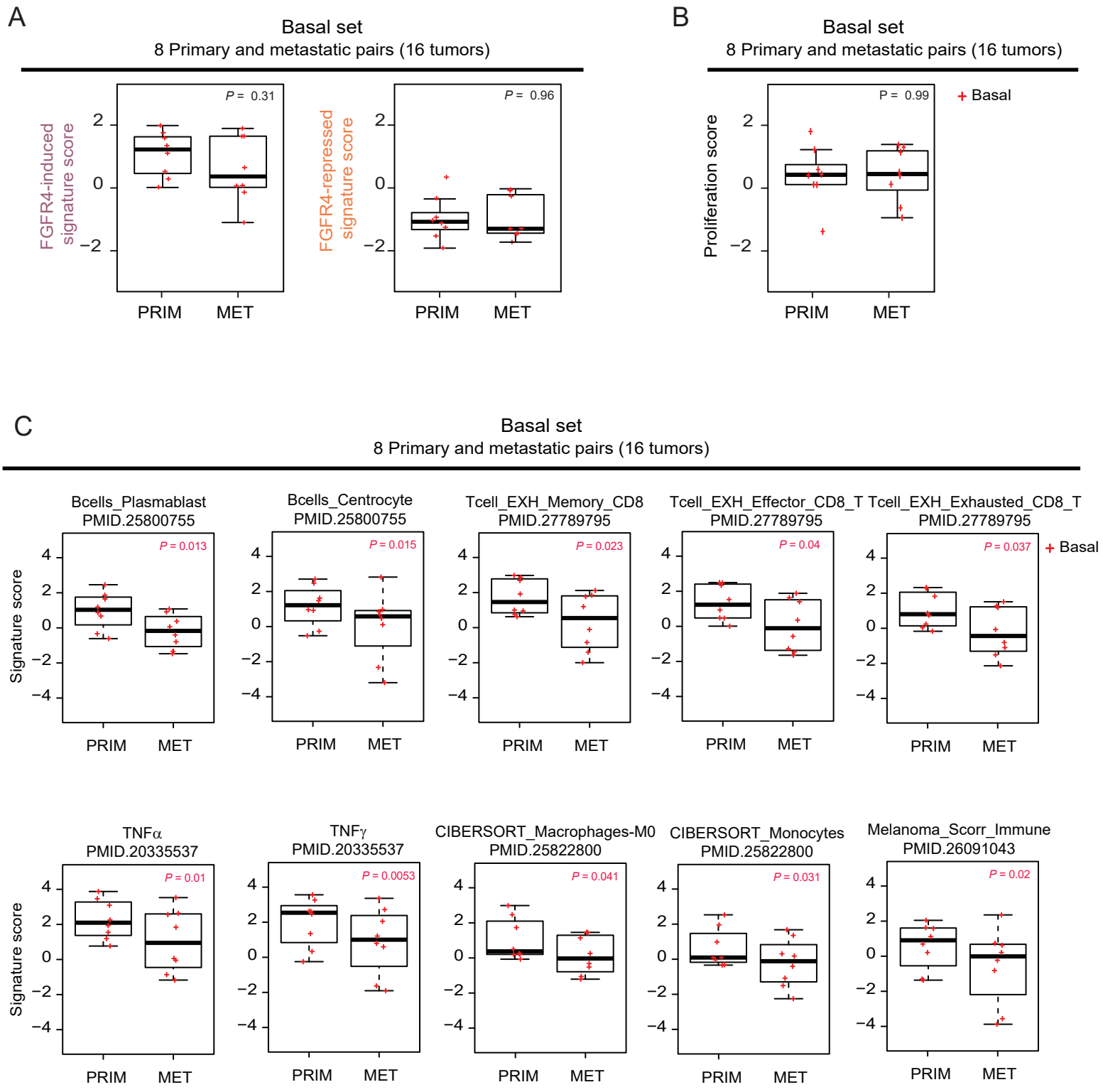

Supplemental Figure 10

Supplemental Figure 10. A, Median expression (signature score) of FGFR4-induced and FGFR4-repressed signature in basal primary and metastatic tumors. **B**, Median expression (signature score) of proliferation signature in basal primary and metastatic tumors. **C**, Median expression (signature score) of some representative immune-related signatures in basal primary and metastatic tumors. (LTS: luminal tumor score, PRIM: primary tumor, MET: metastatic tumor). Boxplot displays the median value on each bar, showing the lower and upper quartile range of the data and data outliers. The whiskers represent the interquartile range. Comparisons between two paired groups were performed by paired t-test (two-tailed). Statistically significant values are highlighted in red. Each mark represents the value of a single sample.

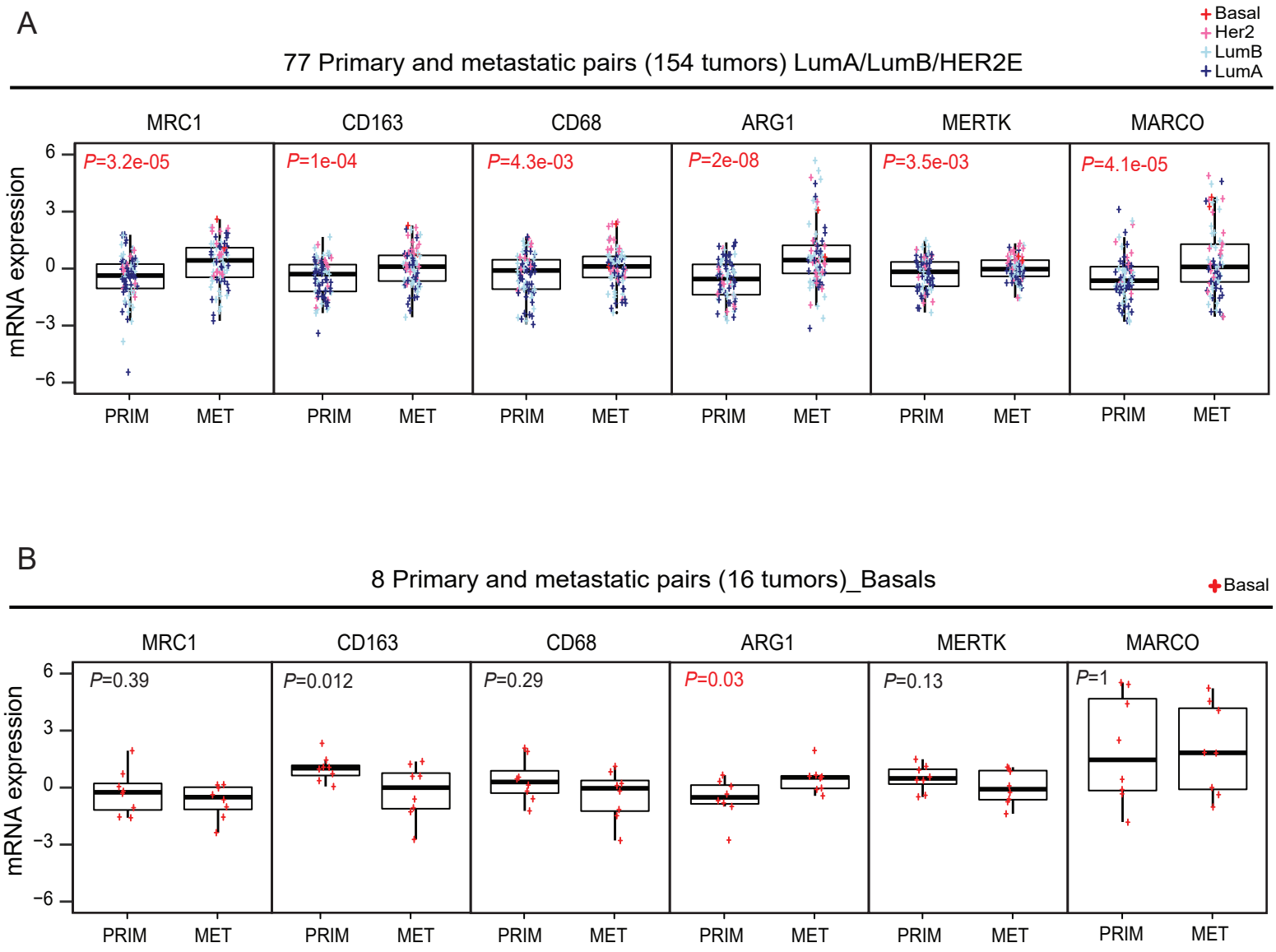

Supplemental Figure 11

Supplemental Figure 11. A, **B**, Comparative mRNA expression of classically M1 (CD68) and alternatively activated M2 macrophages (MRC1, CD163, ARG1, MERTK and MARCO) in (**A**) luminal (**B**) and basal set. Boxplot displays the median value on each bar, showing the lower and upper quartile range of the data and data outliers. The whiskers represent the interquartile range. Each mark represents the value of a single sample. Comparisons between two paired groups were performed by paired t-test (two-tailed). Statistically significant values are highlighted in red. Each mark represents the value of a single sample.

A

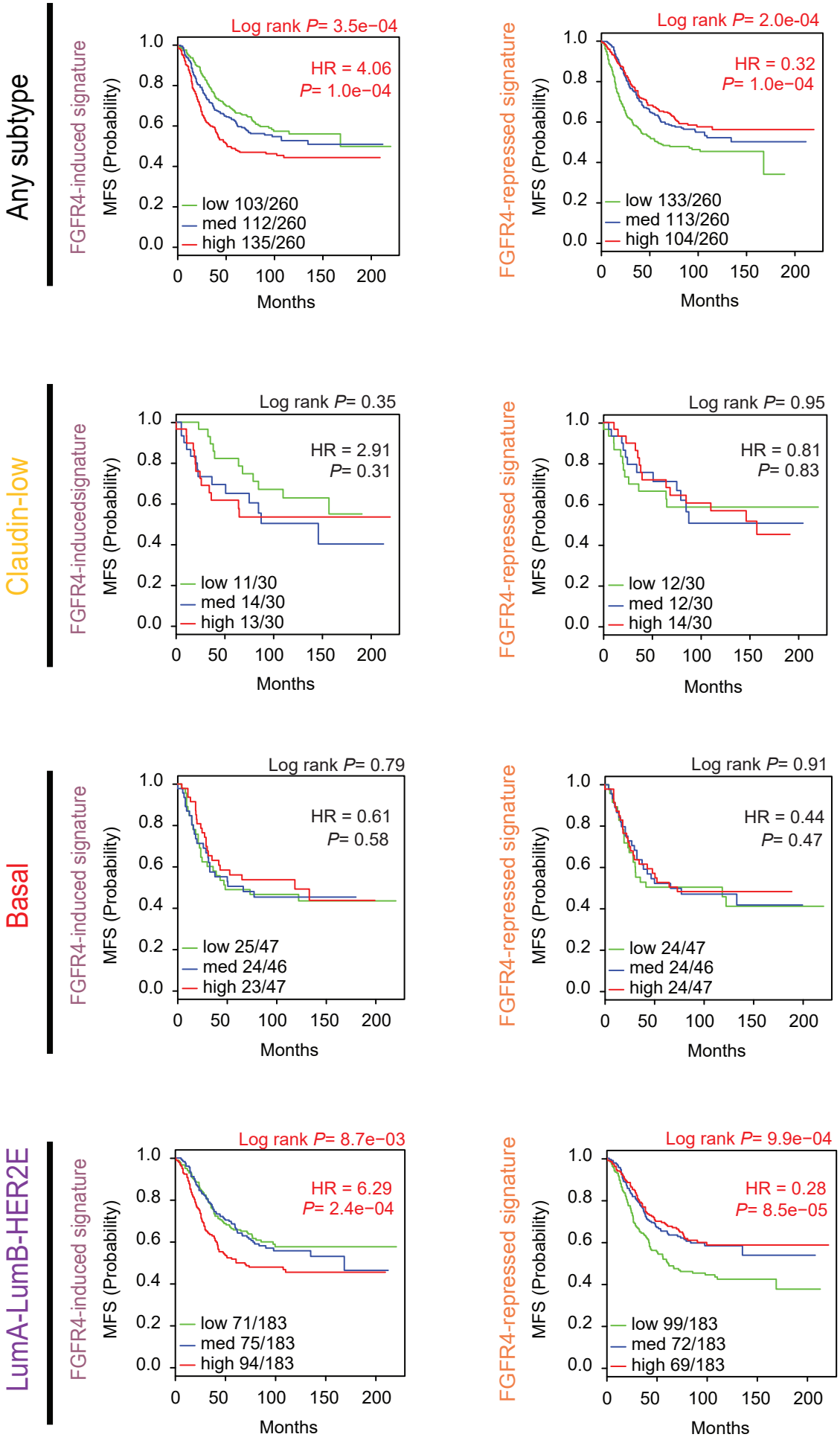

Supplemental Figure 12

Supplemental Figure 12. Univariate analysis in 855 primary tumors with known first site of relapse. A, KM and Cox proportional hazards model analysis of metastasis free survival (MFS) analyzed in 855 primary tumors divided by groups depending on their intrinsic molecular subtype (any subtype, claudin low only, basal only or LumA-LumB-HER2E group). Survival curves differences were calculated by the log-rank test and the estimates of survival probabilities and cumulative hazard with a univariate Cox proportion-hazard model. FGFR4-derived signatures were evaluated as continuous variables and rank-ordered according to the gene FGFR4 signature scores (induced and repressed) in tertiles (low, medium, and high score). HR (Hazard ratio) = 1: No effect. HR < 1: Reduction in the hazard. HR > 1: Increase in Hazard. Statistically significant values are highlighted in red.

A

	Basals		HER2E_LumA_LumB	
	HR	P value	HR	P value
Brain Relapse				
ER (+ vs. −)	1.4E+00	6.4E-01	5.6E-01	3.0E-01
Stage (4+3 vs. 1)	1.4E+01	8.2E-02	1.8E-01	4.3E-01
Stage (2 vs. 1)	2.2E+00	3.9E-01	6.9E-01	5.8E-01
Size	9.9E-01	9.9E-01	1.6E+00	1.7E-01
FGFR4-induced signature	2.1E+00	8.1E-01	8.3E+01	8.5E-03
Lung Relapse				
ER (+ vs. −)	6.9E-01	5.3E-01	4.0E-01	3.1E-02
Stage (4+3 vs. 1)	1.2E+01	3.7E-02	3.2E-07	1.0E+00
Stage (2 vs. 1)	4.3E+00	3.7E-02	2.9E+00	4.3E-02
Size	6.8E-01	2.8E-01	8.1E-01	4.9E-01
FGFR4-induced signature	1.4E+00	8.7E-01	4.0E+01	5.5E-03
Liver Relapse				
ER (+ vs. −)	3.2E-01	3.0E-01	5.5E-01	8.6E-02
Stage (4+3 vs. 1)	5.8E+00	1.4E-01	1.8E-01	1.9E-01
Stage (2 vs. 1)	7.6E-01	6.9E-01	1.1E+00	7.4E-01
Size	1.3E+00	3.9E-01	1.6E+00	1.5E-02
FGFR4-induced signature	7.1E+00	4.3E-01	1.3E+01	1.3E-02
Bone Relapse				
ER (+ vs. −)	1.1E+00	8.9E-01	6.1E-01	4.7E-02
Stage (4+3 vs. 1)	7.9E-01	8.9E-01	1.5E+00	6.2E-01
Stage (2 vs. 1)	4.4E-01	2.3E-01	1.2E+00	4.2E-01
Size	2.0E+00	2.5E-02	1.2E+00	1.2E-01
FGFR4-induced signature	3.6E+00	5.6E-01	1.3E+00	7.4E-01
LN Relapse				
ER (+ vs. −)	2.0E+00	4.7E-01	8.3E-01	8.3E-01
Stage (4+3 vs. 1)	-	-	-	-
Stage (2 vs. 1)	5.5E+08	1.0E+00	1.6E+00	5.3E-01
Size	8.1E-01	7.7E-01	1.5E+00	2.7E-01
FGFR4-induced signature	2.0E+00	8.7E-01	4.9E+00	4.1E-01

B

	Basals		HER2E_LumA_LumB	
	HR	P value	HR	P value
Brain Relapse				
ER (+ vs. −)	2.58E+00	2.36E-01	5.44E-01	2.55E-01
Stage (4+3 vs. 1)	1.54E+01	5.27E-02	2.63E-01	5.62E-01
Stage (2 vs. 1)	2.66E+00	2.97E-01	6.74E-01	5.66E-01
Size	9.22E-01	8.23E-01	1.57E+00	1.84E-01
FGFR4-repressed signature	1.07E-02	1.45E-01	1.30E-02	4.08E-03
Lung Relapse				
ER (+ vs. −)	9.15E-01	8.94E-01	3.24E-01	7.22E-03
Stage (4+3 vs. 1)	1.10E+01	3.82E-02	4.10E-07	9.97E-01
Stage (2 vs. 1)	4.41E+00	3.47E-02	2.97E+00	4.09E-02
Size	6.65E-01	2.52E-01	8.37E-01	5.59E-01
FGFR4-repressed signature	1.65E-01	4.20E-01	1.44E-01	1.07E-01
Liver Relapse				
ER (+ vs. −)	2.89E-01	2.60E-01	4.64E-01	2.35E-02
Stage (4+3 vs. 1)	6.29E+00	1.28E-01	2.18E-01	2.42E-01
Stage (2 vs. 1)	7.68E-01	6.99E-01	1.15E+00	7.20E-01
Size	1.23E+00	4.56E-01	1.57E+00	1.53E-02
FGFR4-repressed signature	3.85E-01	7.14E-01	2.22E-01	9.03E-02
Bone Relapse				
ER (+ vs. −)	8.43E-01	7.86E-01	6.31E-01	5.98E-02
Stage (4+3 vs. 1)	7.22E-01	8.45E-01	1.57E+00	5.78E-01
Stage (2 vs. 1)	4.24E-01	2.19E-01	1.22E+00	4.26E-01
Size	2.04E+00	2.33E-02	1.22E+00	1.31E-01
FGFR4-repressed signature	2.26E+00	6.73E-01	6.25E-01	3.98E-01
LN Relapse				
ER (+ vs. −)	1.46E+01	9.21E-02	8.93E-01	8.87E-01
Stage (4+3 vs. 1)	-	-	-	-
Stage (2 vs. 1)	7.51E+08	9.99E-01	1.59E+00	5.55E-01
Size	5.44E-01	4.19E-01	1.45E+00	3.33E-01
FGFR4 -epressed signature	8.74E-04	1.58E-01	1.15E-01	1.59E-01

Supplemental Figure 13

Supplemental Figure 13. Multivariate analysis among all patients with known first site of relapse. A, Cox proportional hazards model analysis of metastasis free survival (MFS) analyzed in 855 primary tumors divided by groups depending of their intrinsic molecular subtype (Basal only or LumA-LumB-HER2E group). Size, FGFR4 (**A**) induced or (**B**) repressed signatures were evaluated as continuous variables. HR (Hazard ratio) = 1: No effect. HR < 1: Reduction in the hazard. HR > 1: Increase in Hazard. Statistically significant values are highlighted in red.

3. References

1. Usary J, Zhao W, Darr D, Roberts PJ, Liu M, Balletta L, Karginova O, Jordan J, Combest A, Bridges A, et al. Predicting drug responsiveness in human cancers using genetically engineered mice. *Clin Cancer Res.* 2013;19(17):4889-99.
2. Cox J, and Mann M. MaxQuant enables high peptide identification rates, individualized p.p.b.-range mass accuracies and proteome-wide protein quantification. *Nature Biotechnology.* 2008;26(12):1367-72.
3. Johnson WE, Li C, and Rabinovic A. Adjusting batch effects in microarray expression data using empirical Bayes methods. *Biostatistics.* 2007;8(1):118-27.
4. Microarray SSAo. http://www-stat.stanford.edu/%7Etibs/SAM.
5. Tusher VG, Tibshirani R, and Chu G. Significance analysis of microarrays applied to the ionizing radiation response. *Proc Natl Acad Sci U S A.* 2001;98(9):5116-21.
6. Hu Z, Troester M, and Perou CM. High reproducibility using sodium hydroxide-stripped long oligonucleotide DNA microarrays. *Biotechniques.* 2005;38(1):121-4.
7. Cancer Genome Atlas Research N. Integrated genomic analyses of ovarian carcinoma. *Nature.* 2011;474(7353):609-15.
8. Hoadley KA, Weigman VJ, Fan C, Sawyer LR, He X, Troester MA, Sartor CI, Rieger-House T, Bernard PS, Carey LA, et al. EGFR associated expression profiles vary with breast tumor subtype. *BMC Genomics.* 2007;8(258.
9. Nandi S, Guzman RC, and Yang J. Hormones and mammary carcinogenesis in mice, rats, and humans: a unifying hypothesis. *Proc Natl Acad Sci U S A.* 1995;92(9):3650-7.
10. Stuart T, Butler A, Hoffman P, Hafemeister C, Papalexi E, Mauck WM, 3rd, Hao Y, Stoeckius M, Smibert P, and Satija R. Comprehensive Integration of Single-Cell Data. *Cell.* 2019;177(7):1888-902 e21.
11. DePasquale EAK, Schnell DJ, Van Camp PJ, Valiente-Alandi I, Blaxall BC, Grimes HL, Singh H, and Salomonis N. DoubletDecon: Deconvoluting Doublets from Single-Cell RNA-Sequencing Data. *Cell Rep.* 2019;29(6):1718-27 e8.
12. Alzubi MA, Turner TH, Olex AL, Sohal SS, Tobin NP, Recio SG, Bergh J, Hatschek T, Parker JS, Sartorius CA, et al. Separation of breast cancer and organ microenvironment transcriptomes in metastases. *Breast Cancer Res.* 2019;21(1):36.
13. de Duenas EM, Hernandez AL, Zotano AG, Carrion RM, Lopez-Muniz JI, Novoa SA, Rodriguez AL, Fidalgo JA, Lozano JF, Gasion OB, et al. Prospective evaluation of the conversion rate in the receptor status between primary breast cancer and metastasis: results from the GEICAM 2009-03 ConvertHER study. *Breast Cancer Res Treat.* 2014;143(3):507-15.
14. Cejalvo JM, Martinez de Duenas E, Galvan P, Garcia-Recio S, Burgues Gasion O, Pare L, Antolin S, Martinello R, Blancas I, Adamo B, et al. Intrinsic Subtypes and Gene Expression Profiles in Primary and Metastatic Breast Cancer. *Cancer Res.* 2017;77(9):2213-21.
15. Ciriello G, Gatza ML, Beck AH, Wilkerson MD, Rhie SK, Pastore A, Zhang H, McLellan M, Yau C, Kandoth C, et al. Comprehensive Molecular Portraits of Invasive Lobular Breast Cancer. *Cell.* 2015;163(2):506-19.

16. Dobin A, Davis CA, Schlesinger F, Drenkow J, Zaleski C, Jha S, Batut P, Chaisson M, and Gingeras TR. STAR: ultrafast universal RNA-seq aligner. *Bioinformatics.* 2013;29(1):15-21.
17. Patro R, Duggal G, Love MI, Irizarry RA, and Kingsford C. Salmon provides fast and bias-aware quantification of transcript expression. *Nat Methods.* 2017;14(4):417-9.
18. Bullard JH, Purdom E, Hansen KD, and Dudoit S. Evaluation of statistical methods for normalization and differential expression in mRNA-Seq experiments. *BMC bioinformatics.* 2010;11(1):94.
19. de Hoon MJL, Imoto S, Nolan J, and Miyano S. Open source clustering software. *Bioinformatics.* 2004;20(9):1453-4.
20. Hastie T, Tibshirani R, Sherlock G, Eisen M, Brown P, and Botstein D. 1999.
21. Eisen MB, Spellman PT, Brown PO, and Botstein D. Cluster analysis and display of genome-wide expression patterns. *Proc Natl Acad Sci U S A.* 1998;95(25):14863-8.
22. Eisen MB, and Brown PO. DNA arrays for analysis of gene expression. *Methods in enzymology.* 1999;303(179-205.
23. Li S, Shen D, Shao J, Crowder R, Liu W, Prat A, He X, Liu S, Hoog J, Lu C, et al. Endocrine-therapy-resistant ESR1 variants revealed by genomic characterization of breast-cancer-derived xenografts. *Cell reports.* 2013;4(6):1116-30.
24. Huang KL, Li S, Mertins P, Cao S, Gunawardena HP, Ruggles KV, Mani DR, Clauser KR, Tanioka M, Usary J, et al. Proteogenomic integration reveals therapeutic targets in breast cancer xenografts. *Nat Commun.* 2017;8(14864.
25. Parker JS, Mullins M, Cheang MC, Leung S, Voduc D, Vickery T, Davies S, Fauron C, He X, Hu Z, et al. Supervised risk predictor of breast cancer based on intrinsic subtypes. *J Clin Oncol.* 2009;27(
26. Prat A, Karginova O, Parker JS, Fan C, He X, Bixby L, Harrell JC, Roman E, Adamo B, Troester M, et al. Characterization of cell lines derived from breast cancers and normal mammary tissues for the study of the intrinsic molecular subtypes. *Breast cancer research and treatment.* 2013;142(2):237-55.
27. Harrell JC, Prat A, Parker JS, Fan C, He X, Carey L, Anders C, Ewend M, and Perou CM. Genomic analysis identifies unique signatures predictive of brain, lung, and liver relapse. *Breast Cancer Res Treat.* 2012;132(2):523-35.
28. Prat A, Parker J, Karginova O, Fan C, Livasy C, and Herschkowitz JI. Phenotypic and molecular characterization of the claudin-low intrinsic subtype of breast cancer. *Breast Cancer Res.* 2010;12(
29. Fan C, Prat A, Parker J, Liu Y, Carey LA, and Troester MA. Building prognostic models for breast cancer patients using clinical variables and hundreds of gene expression signatures. *BMC Med Genomics.* 2011;4(
30. Gatza ML, Silva GO, Parker JS, Fan C, and Perou CM. An integrated genomics approach identifies drivers of proliferation in luminal-subtype human breast cancer. *Nat Genet.* 2014;46(10):1051-9.
31. Liberzon A, Birger C, Thorvaldsdottir H, Ghandi M, Mesirov JP, and Tamayo P. The Molecular Signatures Database (MSigDB) hallmark gene set collection. *Cell Syst.* 2015;1(6):417-25.
32. Broz ML, Binnewies M, Boldajipour B, Nelson AE, Pollack JL, Erle DJ, Barczak A, Rosenblum MD, Daud A, Barber DL, et al. Dissecting the Tumor Myeloid Compartment

Reveals Rare Activating Antigen-Presenting Cells Critical for T Cell Immunity. *Cancer Cell.* 2014;26(6):938.
33. Prat A, Lluch A, Turnbull AK, Dunbier AK, Calvo L, Albanell J, de la Haba-Rodríguez J, Arcusa A, Chacón JI, Sánchez-Rovira P, et al. A PAM50-Based Chemoendocrine Score for Hormone Receptor-Positive Breast Cancer with an Intermediate Risk of Relapse. *Clinical cancer research : an official journal of the American Association for Cancer Research.* 2017;23(12):3035-44.
34. Paik S, Shak S, Tang G, Kim C, Baker J, Cronin M, Baehner FL, Walker MG, Watson D, Park T, et al. A Multigene Assay to Predict Recurrence of Tamoxifen-Treated, Node-Negative Breast Cancer. *New England Journal of Medicine.* 2004;351(27):2817-26.
35. D'Arcy M, Fleming J, Robinson WR, Kirk EL, Perou CM, and Troester MA. Race-associated biological differences among Luminal A breast tumors. *Breast cancer research and treatment.* 2015;152(2):437-48.
36. Wilkerson MD, Schallheim JM, Hayes DN, Roberts PJ, Bastien RRL, Mullins M, Yin X, Miller CR, Thorne LB, Geiersbach KB, et al. Prediction of lung cancer histological types by RT-qPCR gene expression in FFPE specimens. *The Journal of molecular diagnostics : JMD.* 2013;15(4):485-97.
37. Wilkerson MD, Yin X, Hoadley KA, Liu Y, Hayward MC, Cabanski CR, Muldrew K, Miller CR, Randell SH, Socinski MA, et al. Lung squamous cell carcinoma mRNA expression subtypes are reproducible, clinically important, and correspond to normal cell types. *Clinical cancer research : an official journal of the American Association for Cancer Research.* 2010;16(19):4864-75.
38. Minn AJ, Gupta GP, Siegel PM, Bos PD, Shu W, Giri DD, Viale A, Olshen AB, Gerald WL, and Massagué J. Genes that mediate breast cancer metastasis to lung. *Nature.* 2005;436(7050):518-24.
39. Wilkerson MD, Yin X, Walter V, Zhao N, Cabanski CR, Hayward MC, Miller CR, Socinski MA, Parsons AM, Thorne LB, et al. Differential pathogenesis of lung adenocarcinoma subtypes involving sequence mutations, copy number, chromosomal instability, and methylation. *PloS one.* 2012;7(5):e36530-e.
40. Chang HY, Nuyten DSA, Sneddon JB, Hastie T, Tibshirani R, Sørlie T, Dai H, He YD, van't Veer LJ, Bartelink H, et al. Robustness, scalability, and integration of a wound-response gene expression signature in predicting breast cancer survival. *Proceedings of the National Academy of Sciences of the United States of America.* 2005;102(10):3738-43.
41. Huang F, Reeves K, Han X, Fairchild C, Platero S, Wong TW, Lee F, Shaw P, and Clark E. Identification of candidate molecular markers predicting sensitivity in solid tumors to dasatinib: rationale for patient selection. *Cancer research.* 2007;67(5):2226-38.
42. Chi J-T, Wang Z, Nuyten DSA, Rodriguez EH, Schaner ME, Salim A, Wang Y, Kristensen GB, Helland A, Børresen-Dale A-L, et al. Gene expression programs in response to hypoxia: cell type specificity and prognostic significance in human cancers. *PLoS medicine.* 2006;3(3):e47-e.
43. Liu R, Wang X, Chen GY, Dalerba P, Gurney A, Hoey T, Sherlock G, Lewicki J, Shedden K, and Clarke MF. The Prognostic Role of a Gene Signature from Tumorigenic Breast-Cancer Cells. *New England Journal of Medicine.* 2007;356(3):217-26.

44. van 't Veer LJ, Dai H, van de Vijver MJ, He YD, Hart AAM, Mao M, Peterse HL, van der Kooy K, Marton MJ, Witteveen AT, et al. Gene expression profiling predicts clinical outcome of breast cancer. *Nature.* 2002;415(530.
45. Parker JS, Mullins M, Cheang MCU, Leung S, Voduc D, Vickery T, Davies S, Fauron C, He X, Hu Z, et al. Supervised risk predictor of breast cancer based on intrinsic subtypes. *Journal of clinical oncology : official journal of the American Society of Clinical Oncology.* 2009;27(8):1160-7.
46. Oh DS, Troester MA, Usary J, Hu Z, He X, Fan C, Wu J, Carey LA, and Perou CM. Estrogen-Regulated Genes Predict Survival in Hormone Receptor–Positive Breast Cancers. *Journal of Clinical Oncology.* 2006;24(11):1656-64.
47. Ciriello G, Gatza ML, Beck AH, Wilkerson MD, Rhie SK, Pastore A, Zhang H, McLellan M, Yau C, Kandoth C, et al. Comprehensive Molecular Portraits of Invasive Lobular Breast Cancer. *Cell.* 2015;163(2):506-19.
48. Troester MA, Herschkowitz JI, Oh DS, He X, Hoadley KA, Barbier CS, and Perou CM. Gene expression patterns associated with p53 status in breast cancer. *BMC cancer.* 2006;6(276-.
49. Saal LH, Johansson P, Holm K, Gruvberger-Saal SK, She Q-B, Maurer M, Koujak S, Ferrando AA, Malmström P, Memeo L, et al. Poor prognosis in carcinoma is associated with a gene expression signature of aberrant PTEN tumor suppressor pathway activity. *Proceedings of the National Academy of Sciences of the United States of America.* 2007;104(18):7564-9.
50. Julka PK, Chacko RT, Nag S, Parshad R, Nair A, Oh DS, Hu Z, Koppiker CB, Nair S, Dawar R, et al. A phase II study of sequential neoadjuvant gemcitabine plus doxorubicin followed by gemcitabine plus cisplatin in patients with operable breast cancer: prediction of response using molecular profiling. *British journal of cancer.* 2008;98(8):1327-35.
51. Cancer Genome Atlas N. Genomic Classification of Cutaneous Melanoma. *Cell.* 2015;161(7):1681-96.
52. Liberzon A, Subramanian A, Pinchback R, Thorvaldsdottir H, Tamayo P, and Mesirov JP. Molecular signatures database (MSigDB) 3.0. *Bioinformatics.* 2011;27(12):1739-40.
53. Ashburner M, Ball CA, Blake JA, Botstein D, Butler H, Cherry JM, Davis AP, Dolinski K, Dwight SS, Eppig JT, et al. Gene ontology: tool for the unification of biology. The Gene Ontology Consortium. *Nat Genet.* 2000;25(1):25-9.
54. Kim S, Scheffler K, Halpern AL, Bekritsky MA, Noh E, Källberg M, Chen X, Kim Y, Beyter D, Krusche P, et al. Strelka2: fast and accurate calling of germline and somatic variants. *Nature Methods.* 2018;15(8):591-4.
55. Mose LE, Perou CM, and Parker JS. Improved indel detection in DNA and RNA via realignment with ABRA2. 2019.
56. Danecek P, Auton A, Abecasis G, Albers CA, Banks E, DePristo MA, Handsaker RE, Lunter G, Marth GT, Sherry ST, et al. The variant call format and VCFtools. *Bioinformatics (Oxford, England).* 2011;27(15):2156-8.
57. McLaren W, Gil L, Hunt SE, Riat HS, Ritchie GRS, Thormann A, Flicek P, and Cunningham F. The Ensembl Variant Effect Predictor. *Genome Biology.* 2016;17(1):122.
58. Harsha B, Kok CY, Cole CG, Beare D, Dawson E, Boutselakis H, Jubb H, Tate J, Ponting L, Jia M, et al. COSMIC: somatic cancer genetics at high-resolution. *Nucleic Acids Research.* 2016;45(D1):D777-D83.

59. . COSMIC (Catalogue of somatic mutations in cancer). cancer.sanger.ac.uk.
60. Karczewski KJ, Francioli LC, Tiao G, Cummings BB, Alföldi J, Wang Q, Collins RL, Laricchia KM, Ganna A, Birnbaum DP, et al. Variation across 141,456 human exomes and genomes reveals the spectrum of loss-of-function intolerance across human protein-coding genes. *bioRxiv.* 2019:531210.
61. Lek M, Karczewski KJ, Minikel EV, Samocha KE, Banks E, Fennell T, O'Donnell-Luria AH, Ware JS, Hill AJ, Cummings BB, et al. Analysis of protein-coding genetic variation in 60,706 humans. *Nature.* 2016;536(285.
62. Li H. Aligning sequence reads, clone sequences and assembly contigs with BWA-MEM. 2013.
63. Tischler G, and Leonard S. biobambam: tools for read pair collation based algorithms on BAM files. *Source code for biology and medicine.* 2014;9(13-.
64. Cancer Genome Atlas N, Koboldt DC, Fulton RS, McLellan MD, Schmidt H, Kalicki-Veizer J, McMichael JF, Fulton LL, Dooling DJ, Ding L, et al. Comprehensive molecular portraits of human breast tumours. *Nature.* 2012;490(7418):61-70.
65. Xia Y, Fan C, Hoadley KA, Parker JS, and Perou CM. Genetic determinants of the molecular portraits of epithelial cancers. *Nature Communications.* 2019;10(1):5666.
66. Liu ML, Shibata MA, Von Lintig FC, Wang W, Cassenaer S, Boss GR, and Green JE. Haploid loss of Ki-ras delays mammary tumor progression in C3 (1)/SV40 Tag transgenic mice. *Oncogene.* 2001;20(16):2044-9.
67. Curtis C, Shah SP, Chin S-F, Turashvili G, Rueda OM, Dunning MJ, Speed D, Lynch AG, Samarajiwa S, Yuan Y, et al. The genomic and transcriptomic architecture of 2,000 breast tumours reveals novel subgroups. *Nature.* 2012;486(7403):346-52.
68. Prat A, Carey LA, Adamo B, Vidal M, Tabernero J, Cortés J, Parker JS, Perou CM, and Baselga J. Molecular Features and Survival Outcomes of the Intrinsic Subtypes Within HER2-Positive Breast Cancer. *JNCI: Journal of the National Cancer Institute.* 2014;106(8):dju152-dju.
69. Harrell JC, Prat A, Parker JS, Fan C, He X, Carey L, Anders C, Ewend M, and Perou CM. Genomic analysis identifies unique signatures predictive of brain, lung, and liver relapse. *Breast Cancer Res Treat.* 2011;132(
70. Hatzis C, Pusztai L, Valero V, Booser DJ, Esserman L, and Lluch A. A genomic predictor of response and survival following taxane-anthracycline chemotherapy for invasive breast cancer. *JAMA.* 2011;305(
71. Nielsen TO, Parker JS, Leung S, Voduc D, Ebbert M, and Vickery T. A comparison of PAM50 intrinsic subtyping with immunohistochemistry and clinical prognostic factors in tamoxifen-treated estrogen receptor-positive breast cancer. *Clin Cancer Res.* 2010;16(